A Microsystems Approach for Drug Assessment

Sepeedah Soltanian-Zadeh

Thesis submitted to the faculty of the Virginia Polytechnic Institute and State University in partial fulfillment of the requirements for the degree of

Master of Science

In

Electrical Engineering

Masoud Agah, Chair

Amy Pruden-Bagchi

Wei Zhou

July 18th, 2016

Blacksburg, VA

Keywords: Micro Electrical Mechanical Systems (MEMS), Drug Assessment, Breast Cancer, Migration Assay, Dielectrophoresis

A Microsystems Approach for Drug Assessment

Sepeedah Soltanian-Zadeh

ABSTRACT

Cancer metastasis, the departure of cancer cells from the primary tumors and their spread to distant sites, is responsible for 90% of cancer related deaths. Thus, understanding the initial process which leads to cancer metastasis in the later stage and stopping the spread in the initial stage deems necessary. In spite of significant progress in diagnosis and treatment, there is still the need for robust and easy to use drug assessment methods. In this work we present two approaches for this purpose: a microengineered Boyden chamber, and a dielectrophoresis-based platform for cell characterization and drug assessment. Using these methods, we characterize the drug response of breast cancer, which is the second most common type of cancer among US women.

The micorengineered Boyden chamber we designed in this work is made of a silicon-based transmigration well with a 30μm-thick membrane and 8μm pores. This platform includes a deep microfluidic channel on the back-side sealed with a glass wafer. Using this platform, the migratory behavior of highly metastatic breast cancer cells, MDA-MB231, is tested under different drug treatment conditions. The second platform, the off-chip passivated electrode insulator-based dielectrophoresis (OπDEP) device, has been used to first distinguish between different breast cancer cell lines namely LCC1/MCF7, LCC9/MCF7, MCF7, and MDA-MB231, and also to probe the effect of different drug treatments on the cells. These versatile platforms will enable the enhanced integration with other technologies and running multiple assays simultaneously. Moreover, the methods presented show potential for next generation drug discovery and patient follow up purposes.

To My Family

Acknowledgements

This work reflects my short but yet valuable experience at Virginia Tech which would not have been possible without the help of many. First and foremost, I would like to express my deepest gratitude towards my adviser, Dr. Masoud Agah, who has supported me along this journey. Without his help none of this work would have been possible. I would also like to thank my committee members Dr. Amy Pruden and Dr. Wei Zhou who have been very supportive throughout the course of this work and provided valuable feedback.

The presented work in this thesis has been the result of two very productive and successful collaborations. The first part of this work was initiated by Dr. Yahya Hosseini during his PhD research at the VT MEMS lab and continued as a collaborative effort with him. I would like to acknowledge his innovative technical contribution to this study. The second half of this work was a collaboration with Dr. Ayesha Shajahan-Haq at the Lombardi Cancer Center at Georgetown University and also Ms. Kruthika Kikkeri at the VT MEMS lab. I would like to thank all of the mentioned collaborators for their valuable work and their help throughout this research, without them none of this would have been possible. Working with these people taught me the value of collaboration and team work in research. I also would like to acknowledge Dr. Phillip Zellner's work and technical innovation for the platform we used in the second half of the study, since the mentioned platform is mainly based on his work during his PhD studies at the VT MEMS lab.

I would like to thank other past and current members of the VT MEMS lab, Dr. Vaishnavi Srinivasaraghavan for her valuable information, her patience, and her willingness to help anyone who needed help in the lab. Also Dr. Jeannine Stroble, Dr. Hesam Babahosseini, Dr. Muhammad Akbar, Ms. Sarah El-Helw, and Mr. Parham Ghaessemi who helped me when needed and made the lab a better place to work. Furthermore, I would like to thank Mr. Don Leber at the MicrON facility for his help and knowledge in the cleanroom, and Ms. Kathy Lowe at the VT college of Veterinary Medicine for her help in morphological characterizations.

Last and most importantly, I would like to thank my family for their continuous love and support. My father whose continuous style of work taught me to never quite. My mother who showed me anything in life is possible if you are willing to do it. And my sisters who have offered me not only support during my life, but also valuable friendships I cannot find elsewhere.

Sepeedah Soltanian-Zadeh
July 2016

Table of Contents

List of Figures

List of Tables

Chapter 1. Introduction

1.1 Significance of Miniaturization in Next Generation Drug Discovery

The selection of an effective molecule to act as a drug for a certain disease is a timely and laborious process which requires the testing of the chosen molecule *in vitro* at the first level, *in vivo* at the second level, and clinical trials thereafter. This process is limited by the technological advances in the handling of liquid samples and available high through put processes and analyses. Miniaturization systems or microsystems can simplify this process and lead to increased speed and automation opportunities. Microsystems and microfluidic platform provide various advantages such as serial processing on a single platform and also the possibility of parallelization in order to increase throughput [1]. These advantages are summarized in Figure 1-1.

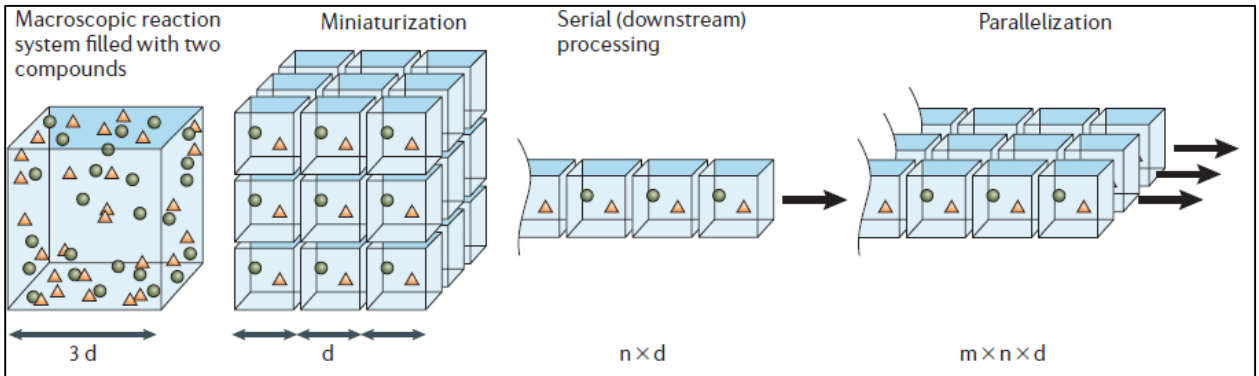

Parameter	Macroscopic example	Factor change	Microscopic example
Length of edge	1 mm	d	1 µm
Surface	1 mm²	d²	1 µm²
Volume	1 µl	d³	1 fl
Number of molecules	10^9	d³	1
Diffusion time over d (D = 10^{-6} cm²s⁻¹)	15 min	d²	1 ms
Example: in flowing systems			
Linear flow rate	1 µm/s	d	1 mm/s
Separation time	10^5 s (>1 day)*	d²	100 ms
Example: in planar array			
Number of volumes per microwell plate	96	d²	10^8

*Typically, for example, high-performance liquid chromatography in packed column.

Figure 1-1 Advantages gained by miniaturization [1]. Reprinted with permission from Nature Publishing Group.

1.2 Drug Assessment in Breast Cancer

Drug discovery for cancer encompasses various experiments and conditions based on the type of cancer and specific type of resistance inherent to each cancer type. The main type of cancer studied in this work is breast cancer. Breast cancer is the leading cause of cancer related death among women aged 20 to 59 years old in the United States [2] and the second leading cause of cancer related deaths among women of all ages, affecting 1.7 million women each year [3]. It is estimated that breast cancer alone will account for 29% of all new cancer diagnosis in 2016 [2]. Breast cancer is unique in the sense that it includes various types of resistance behavior, leading to different clinical treatments and outcomes [4]. Breast cancer is generally categorized in three major types based on immunohistochemical properties: 1) hormone receptor (HR)-positive for estrogen (ER) and progesterone (PR) hormones, 2) human epidermal growth factor receptor 2 positive ($HER\text{-}2^{+}$) and, 3) triple-negative breast cancer (TNBC) [3]. HR^{+} type accounts for approximately 85% of all breast cancers and has the best prognosis among all types. Endocrine therapies such as tamoxifen and aromatase inhibitors (AI) are used for treatment of this type. Approximately 15% of breast cancer are TNBC type which does not over express hormone receptor, therefore rendering targeted hormonal therapies useless and having the worst prognosis [3]. In this regard we introduce two independent micron-scale platforms for the study of the anti-tumor drugs on different types of breast cancer.

The first platform, referred to as the Microengineered Boyden chamber, is mainly focused at drug assessment for TNBC cells such as MDA-MB231 which exhibit high migration and invasion activity. The second platform, referred to as the off-chip passivated insulator based dielectrophoresis (OπDEP), is used to probe the effect of anti-tumor drugs on HR^{+} cancer cells which are less invasive than TNBC cells but may acquire de novo resistance to therapeutic drugs. In the continuing sections we review the background information for these two platforms.

1.3 Cell invasion and Migration

According to the American Cancer Society (ACS), in 2014, more than 1.6 million new cases of cancer were diagnosed only in the United States [5]. Unfortunately, the current standard treatment methods are not effective if the patients are diagnosed at late stages of cancer. With recent advancement in biotechnology, new anti-metastasis drugs have been developed to reduce the risk

of cancer spread throughout the body. Such drugs are currently in human clinical trials and still used in combination with the old treatment techniques. Although the application of the new drugs has been investigational, they are promising to be a safer and non-toxic alternative to the standard chemotherapeutic approaches when their interaction with the extracellular matrix (ECM) and tumorigenic cells is fully understood. In order to better understand the effectiveness of such drugs, in addition to approved, yet complicated and lengthy tests on human subjects, it is necessary to develop tools to perform these studies in a system that closely resembles tumor microenvironments outside human body (*in vitro* micro-devices).

Metastasis is responsible for 90% for cancer death. Metastasis involves the departure of cancer cells from the primary tumors to the spread of cells at the distance sites. As Figure 1-2 shows, in brief, during the metastasis process tumor microenvironment secretes growth factors that leads to formation of new blood vessels nearby the tumor cells (angiogenesis). Then cancer cells invade the surrounding ECM, enter the microvasculature (intravastation), and traverse through the blood stream to reach the tissues at distant sites. At the end, cancer cells exit the microvasculature (extravasation) and establish and proliferate in the new microenvironment, and this cycle may continue [6]. As already described above, metastasis involves multiple processes. However, the initial cell invasion to the ECM and tissue is the main stage where the cancer metastasis is orchestrated. Therefore, understanding the interaction of cells with the microenvironment is an utmost of importance on how it acquires invasive characteristics.

In order to clinically treat cancer, it is important to develop novel anti-metastasis drugs that can prevent the spread of cancer. These candidate drugs can be developed upon our understanding of metastasis mechanism at the very early stage which includes cell migration and invasion of cancer cells through the surrounding ECM. Unfortunately, monitoring the effect of the candidate drugs on inhibiting the cell invasion and angiogenesis is challenging.

Cell invasion and migration have many similarities. Cell migration is prerequisite of cell invasion. In cell migration, ECM is the substrate carrier for cell adhesion and movement. In the process of cell migration, cells polarize and elongate a leading edge toward the migration direction. This tail then applies a traction force on the cell body which produces a gradual cellular movement on the ECM [7]. In cell invasion, cells advance through the ECM which acts as a barrier. Therefore, this process involves degradation or remodeling of ECM to facilitate the cell movement [8].

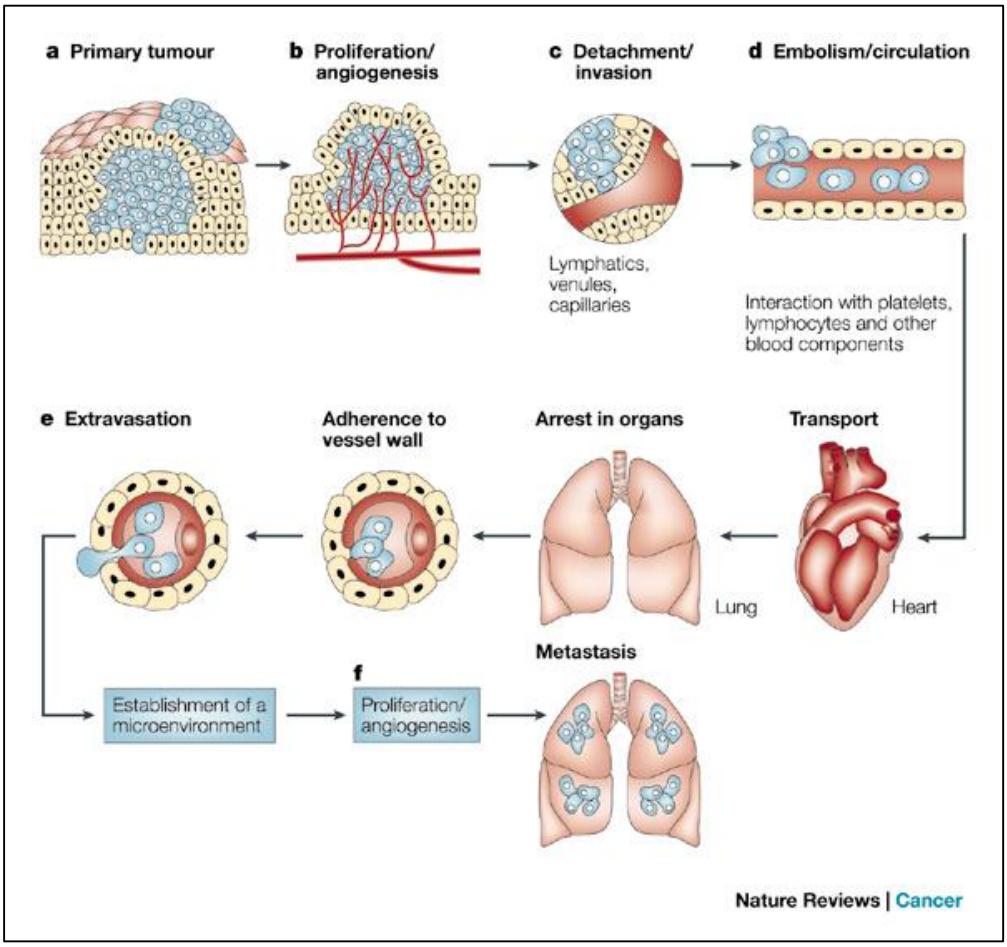

Figure 1-2 (a) Cellular transformation and tumor growth (b) formation of new blood vessels to the tumor sites (c) cancer invasion (d) circulation of tumor cells and reaching to distance sites (e) tumor cells leave the vessels to find new host, and (f) proliferation within the new host and formation of new vascular networks to the tumor sites. This cycle might be repeated. Reprinted with permission from Nature Publishing Group [6].

1.4 *In vitro* Transmigration-invasion Assays

Traditionally, 2-D culture systems were widely used to study the interaction of cells with each other and biochemical reagents in culture plates, culture flasks, and Petri dishes due to ease of use and high viability of cells on 2-D surfaces [9, 10]. However, cells behave on 2-D and 3-D surfaces in many different ways. 3-D scaffolds are more suitable for cells to interact with neighboring cells and ECM in a natural way. 3-D scaffolds can be engineered to contain the same proteins as the native tissues. Their mechanical properties can be tuned to help cells organize themselves and communicate with each other. The role of focal adhesion in cell motility is completely different in

2-D and 3-D systems [11], and cell migration and invasion is a process bounded to a 3-D environment. In this regard, hydrogels have been being used extensively as scaffolds to model ECM as they are water abundant, biocompatible, and their physical and chemical characteristics can be adjusted to create a biologically relevant microenvironment.

The traditional *in vitro* models developed first by Boyden to study transmigration and invasion assays in 2-D typically encompasses a cell culture insert housed inside a culture plate as shown in Figure 1-3. The insert consists of a porous membrane with a predefined size depending on the size of cells to be monitored. Cells are cultured on the insert and the media with chemoattractant of interest (eg, cell media + candidate drug) is added to the culture plate below. The cell migration is characterized by the number of cells passing through the porous membrane. Furthermore, cell invasion assay can be performed by coating a layer of ECM proteins on top of the insert. Such platforms have been developed to classify the invasion rate of lung cancer cells [12], study migration of single tumor cells [13], study the effect of specific proteins on the migration of brain cancer cells [14]. Additionally, similar platforms have been developed to increase and diversify the functionalities of this commercial products. For instance, wound healing assay is utilized to measure the rate of cells can repair a damaged wound [15, 16]. Spheroid migration assay [17, 18] is used to monitor the migration behavior of tumor spheroid clusters on a 2-D surfaces and etc. *In vitro* trans-migration and invasion assays enable the examination of a particular candidate drugs on the cells of interest without the presence of other proteins and cells. These assays are inexpensive, and can be performed easily, in a short period of time and is suitable for high throughput screening. Furthermore, this type of *in vitro* testing can be used to test the validity of some certain drugs prior to animal testing to reduce the quantity of animal suffrages which has raised many ethical questions. However, these platforms are primitive and do not have the complexity of *in vivo* microenvironments in terms of structures, functionalities and fluidic circulations.

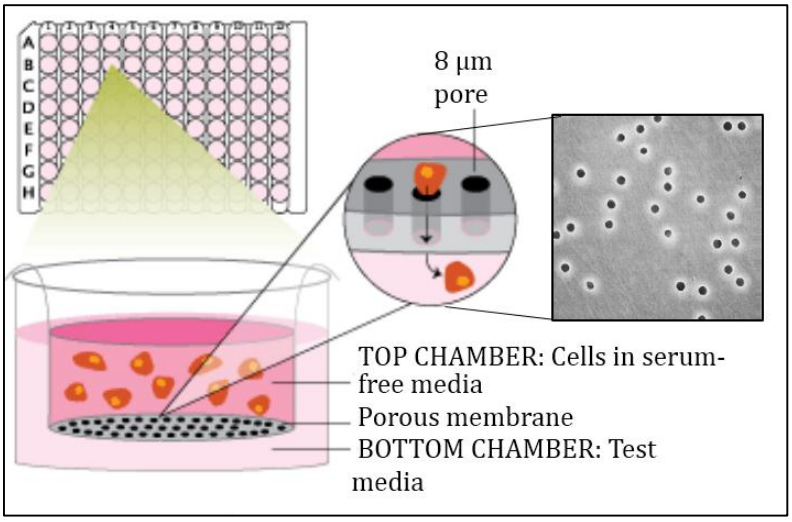

Figure 1-3 Boyden chamber consisting of polymeric membrane insert in a cell culture well plate. Cells are seeded on top of the porous membrane separating the different media conditions. Inset shows the pore structure in the conventional polymeric membranes. Part of image adapted from [19].

With the help of microfabrication techniques and utilizing microfluidics, researchers have been able to extend the applications and complexity of the commercial *in vitro* migration and invasion assays. A microfluidic platform is developed to study the cell invasion of endothelial and cancer cells [20, 21]. As shown in Figure 1-4, this platform consists of two side channels and one central channel which are connected to each other by collagen hydrogel scaffold. Cells are introduced to the central channel and the control and chemoattractant media are introduced to the side channels. This platform enables to study the migratory phenotype of different types of cells by changing the biochemical cues.

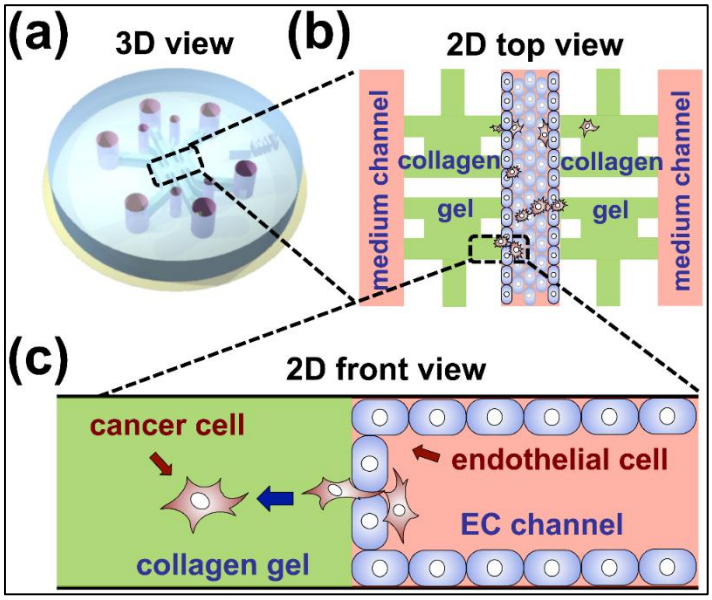

Figure 1-4 (a) Microfluidic system consisting of three independently addressable media channels, separated by chambers into which an ECM-mimicking gel can be injected. (b) Figure shows the inside view of the device with endothelial monolayer (blue) covering the center channel. This channel acts as cell channel where both endothelial cells and cancer cells are introduced to form monolayer and transmigrate respectively. (c) The green region indicates the 3D space filled with collagen gel and the pink regions indicate the channel filled with medium. Cancer cells which adhere to endothelial monolayer can extravasate into the collagen gel region as shown in. Reproduced from [22] (PLOS one).

A multi-layer microfluidic device is developed to model vascular/valvular three- dimensional environment [23]. As shown in Figure 1-5, this platform consists of two overlaying channels separated by a porous membrane. The bottom channel is filled with gelatin methacrylate (gel-MA) co-cultured with valvular interstitial cells (VICs), the top channel provides fluidic access, and the membrane is cultured with vascular endothelial cells. This platform was applied to investigate shear stress-regulated paracrine interactions between valvular endothelial cells and valvular interstitial cells. Several other microfluidic-based prototypes are developed with various functionalities and applications; analyze the specificity of human breast cancer cells to bones in a microenvironment that similar to vascularized osteo-cell microenvironment [24], study the breast cancer progression from early stage non-invasive ductal carcinoma *in situ* (DCIS) to the late stage invasive ductal carcinoma (IDC) [25], study the cell invasion characteristics of breast cancer cells (MCF7) by generating epidermal growth factor (EGF) concentration gradient across the cell channel and suppressing their invasion by an anti-invasion, matrix metalloproteinase inhibitor GM6001 [26], quantify the migration and extravasation phenotype of primary tumor cells such as HepG2, HeLa, and MDA-MB 435S through a series of narrow capillary micro-channels [27].

These platforms mimic the physiological conditions cells undergo in *in vivo* microenvironments by integration of biochemical and biomechanical factors. These conditions permit the study of biological processes such as cell invasion *in vitro*, however lack the cell architecture found within the tissues and organs [28-32].

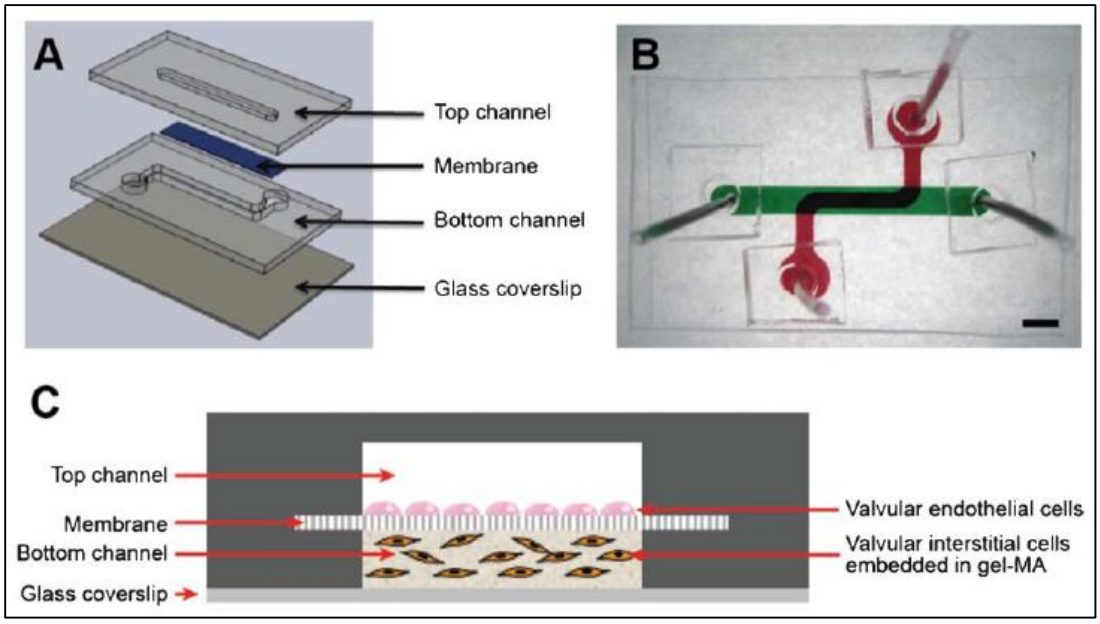

Figure 1-5 (a) Schematic and (b) photograph of bilayer membrane microfluidic device. The scale bar in panel (b) is 5 mm. (c) Cross-sectional schematic illustrating the spatial arrangement of the cells in the device. Reproduced from [23] with permission from Royal Society of Chemistry.

1.5 Dielectrophoresis and Implications in Cellular Samples

Dielectrophoresis (DEP) is the motion of polarizable particles that are suspended in a dielectrically dissimilar media when subjected to a spatially non-uniform electric field [33] Unlike electrophoresis, particles do not need to have any net charge to be effected by DEP. Instead, for a particle to be affected by DEP, it needs to be polarizable. Figure 1-6a illustrates the effect of placing a charged and a neutral particle in a uniform electric field. The charges within the particle align with the electric field, creating an induced dipole. However, the distribution of the positive charges directly mirrors the distribution of negative charges. Thus the net Coulomb force on the neutral particle is zero. In Figure 1-6b a non-uniform electric field is applied to polarizable neutral particles. When the charges within the particles align with the electric field, the charge distributions do not mirror each other, creating a force on the

particles based on their intrinsic properties. This nonzero Coulomb force on an uncharged polarizable particle in a non-uniform field is known as dielectrophoresis.

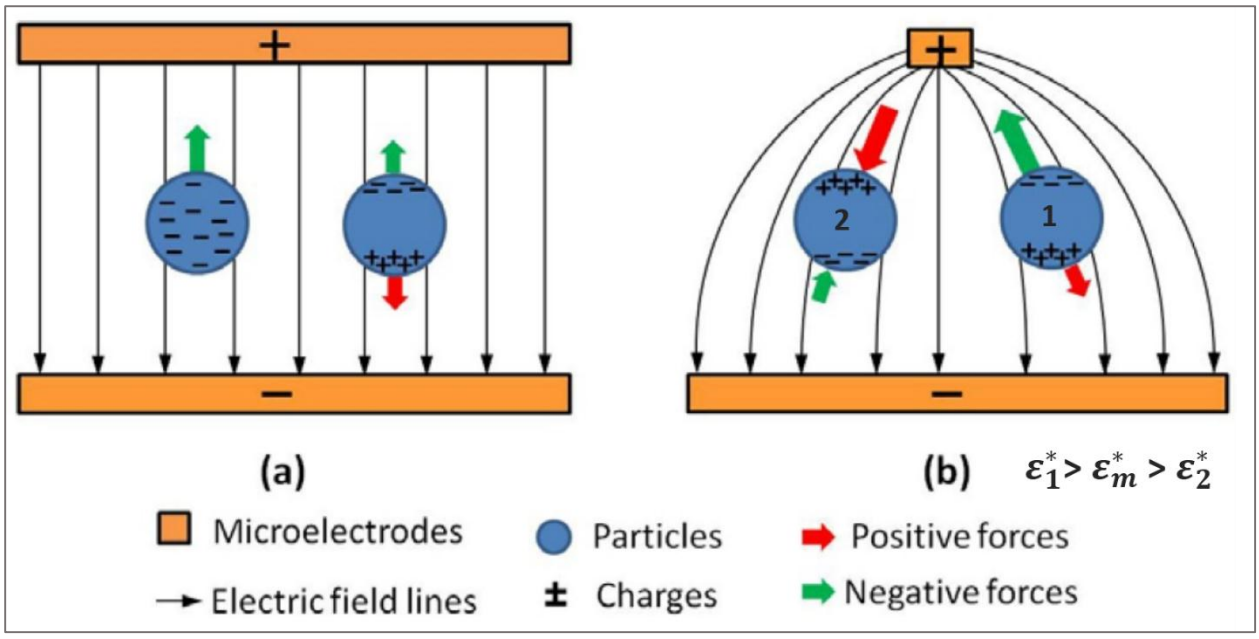

Figure 1-6 Different particles and their varying behavior (a) coulomb force balance for a charged and neutral particle in a uniform electric field, (b) behavior of two dissimilar neutral particles in a non-uniform electric field. Reproduced from [34] with permission from IOP Publishing. All rights reserved. (http://dx.doi.org/10.1088/0022-3727/47/6/063001)

The resulting force felt by the particles is due to an induced dipole as described by the Maxwell-Wagner (MW) they. The dielectrophoretic force on a sphere can be derived directly from the induced dipole model [39, 40]. The time average DEP force felt by a spherical particle suspended in a medium is:

Equation 1-1

$$F_{DEP} = 2\pi R^3 \varepsilon_m Re[f_{CM}] \nabla |E_{RMS}|^2$$

where R is the radius of the particle, ε_m is the permittivity of the medium, E_{RMS} is the local electric field. This equation can be derived theoretically for the case of a homogenous or inhomogeneous sphere [40]. $Re[f_{CM}]$ is the real part of the Clausius-Mossotti factor. The Clausius-Mossotti factor includes complex parameters which can be used to describe a biological cell fit to a multishell model. The factor which is:

Equation 1-2

$$f_{CM} = \left(\varepsilon_p^* - \varepsilon_m^*\right) / \left(\varepsilon_p^* + 2\varepsilon_m^*\right)$$

where ε_p^* and ε_m^* are the complex permittivities of the particle and the medium, respectively. Complex permittivity is defined as:

Equation 1-3

$$\varepsilon^* = \varepsilon + \sigma/(j\omega)$$

where ε and σ are the real permittivity and conductivity, j =sqrt(-1) and ω is the angular frequency of the applied potential signal. For DC-field insulator-based DEP experiments the complex permittivity becomes the low frequency limit of this equation which is simply the conductivity. Thus, the Clausius-Mossotti factor for DC is:

Equation 1-4

$$f_{CM} = \left(\sigma_p^* - \sigma_m^*\right) / \left(\sigma_p^* + 2\sigma_m^*\right)$$

Figure 1-6b also illustrates the consequences of these equations. In this figure an electric field is created by applying a sinusoidal signal with a frequency of ω. Assume that there are two geometrically identical particles 1 and 2 with complex permittivities ε_1^* and ε_2^*, respectfully, suspended in a medium with a complex permittivity ε_m^* such that $\varepsilon_1^* > \varepsilon_m^* > \varepsilon_2^*$. For this situation, $Re[f_{CM}]$ will be positive for particle1, thus p1 will be attracted to the region with the highest electric field gradient. This is known as positive DEP. Conversely, $Re[f_{CM}]$ will be negative for particle2, thus p2 will be repelled from the region with the highest electric field gradient. This is known as negative DEP. Thus the intrinsic properties of the particle play a large role in its response to a non-uniform electric field and how the dielectrophoresis force is applied on the particle.

To explain the response of biological particles to applied electric fields, the shell model of a cell was developed. In the single shell model, a cell is described as a sphere of highly conductive cytoplasm encased by a highly insulating membrane. In order to more accurately model the complex cell structure, the single shell model of the cell can be refined by considering a sphere contained in another sphere [35]. This process can be repeated until the cell's behavior is adequately described and is known as the multishell model (Figure 1-7). The relevant information is conserved each iteration by using "effective" complex parameters to describe particle in the

Clausius-Mossotti factor as described below. While for this work, we will treat all of the particles as spherical, this theory can be extended to nons-pherical particles.

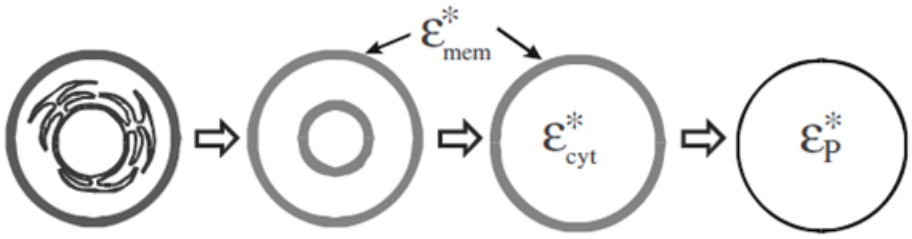

Figure 1-7 Diagram Schematic representation of how a cell can be simplified into a homogenous particle with effective permittivity εp*. Reprinted from [36] with permission from AIP Publishing LLC.

The DEP force magnitudes will be different for particles of different size and material makeup. These differences in particle conductivity and size result in different DEP force magnitudes. This allows for selectivity among particles. In addition, the presence of mobile ions bounded by various dielectric layers leads to different MW relaxation timescales. The result is that the DEP force on a particle is frequency dependent, especially for inhomogeneous particles such as biological cells. As shown in Figure 1-8, there are two cross over frequencies in which the cell and the media have an equivalent complex permittivity. In these cases, no DEP force acts upon the cell and the cell is basically invisible to the electric fields. Changes in the biophysical properties of the cell can cause changes in the cross over frequency making it a valuable tool to monitor changes in the cell.

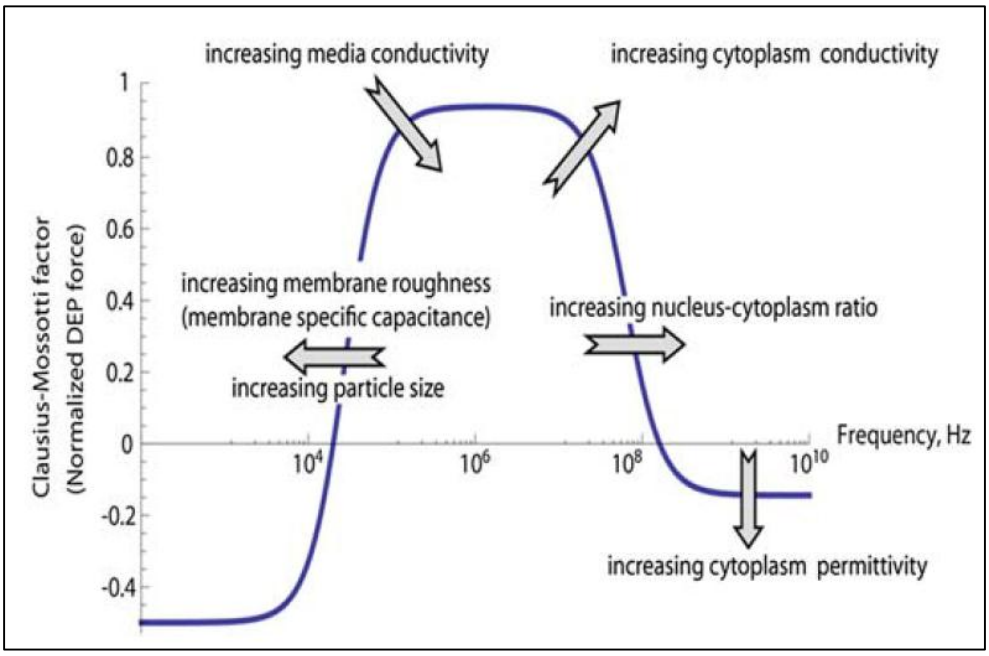

Figure 1-8 Clausius-Mossotti factor for a typical mammalian cell, arrows show this parameter is affected by changes in the cell. Reproduced from [37].

Chapter 2. A Microengineered Boyden Chamber for Cell Migration Analysis

Acknowledgments: This work was initiated by Dr. Yahya Hosseini during his PhD research and continued as a collaborative effort with him. I acknowledge his innovative technical contribution to this study. I also acknowledge the contributions of Dr. Vaishnavi Srinivasaraghavan and Dr. Masoud Agah who are co-authors on the upcoming publication from this work.

2.1 Introduction

Traditionally, 2-D culture systems have been widely used to study the interaction of cells with each other and biochemical reagents in culture plates, culture flasks, and petri dishes due to their ease of use and high viability of cells on 2-D surfaces [9, 10]. The first *in vitro* model developed by Boyden to study transmigration and invasion in 2-D, typically encompasses a cell culture insert housed inside a culture plate. The insert consists of a porous membrane with a predefined pore size depending on the size of cells to be monitored. Such platforms have been developed to investigate the invasion rate of lung cancer cells [12], study single tumor cell migration [13], and examine effect of specific proteins on brain cancer cells [14]. Additionally, similar platforms have been developed to increase and diversify the functionality of commercial products. For instance, the wound healing assay is utilized to measure the rate of cell migration during repair of a damaged wound [15, 16]. Spheroid migration assay [17, 18] is used to monitor the migration behavior of tumor spheroid clusters on 2-D surfaces.

With the help of microfabrication techniques, researchers have been able to miniaturize and build targeted applications for commercial *in vitro* migration and invasion assays. Utilizing soft lithography and gel injection, a microfluidic platform was developed to study the cell invasion of endothelial and cancer cells through a central channel into the side channels loaded with a chemoattractant [20, 21]. A microfluidic device with two overlaying channels separated by a commercially available 1µm-porous membrane was developed to model a vascular/valvular three-dimensional environment [23]. This platform was employed to investigate shear stress-regulated

paracrine interactions between valvular endothelial cells and valvular interstitial cells. Another microfluidic device was developed in PDMS to quantify the migration and extravasation phenotype of primary tumor cells through a series of 2-D planar narrow capillary micro-channels [27]. Several other micro-based Boyden chamber devices have been developed mainly by incorporating a commercially available porous membrane to study cell migratory behaviors [38, 39].

In some of the above instances, like a Boyden chamber, cell channels are separated by a membrane or a gel layer from the chemoattractant channels. The membrane layer is cut from a commercially available transmigration well and incorporated between the custom fabricated source and chemoattractant channels, which reduces the integration capabilities of these systems as well as increases the manual labor required for fabrication. In planar devices with parallel channels, although imaging is facilitated, the throughput of the system is limited to less than two simultaneous assays.

So far, silicon has been the material of choice for micromachining. With the help of lithography and dry etching, a wide variety of structures can be fabricated in a controlled fashion, precisely on silicon substrates. DRIE has been utilized to construct deep trenches, high aspect ratio through-silicon vias [40, 41], arrays of micropillars [42] and nanowires [43]. In this setting, the etch parameters can be adjusted to control the etch rate, etch directionality, scalloping and uniformity [44, 45]. In this report, we take advantage of lithography and DRIE techniques to fabricate a versatile migration assay platform in silicon. The lithography process enables the formation of pores with different sizes and densities across a single membrane which can be used to adjust the diffusion profile. Furthermore, this work utilizes DRIE to fabricate a microfluidics-enabled deep micro-channel with a porous thin-membrane on a single silicon wafer with a high level of control on the membrane-thickness. In the future, we can take advantage of semiconductor processing techniques and silicon's electrical and mechanical properties, to investigate electrode integration for impedance sensing, improved microfluidic circulation and gradient profiles, and high throughput cell migration screening based on different candidate-drug treatment plans.

2.2 Methods

I. Cell preparations

Cell Culture: The metastatic human breast cancer cell line, MDA-MB 231 (a gift from Dr. Ayesha Shajahan-Haq, Lombardi Cancer Center, Georgetown University, Washington, DC) was obtained from American Type Culture Collection (ATCC, VA, USA). Cells were maintained in T-25 flasks in Dulbecco's Modified Eagle's Medium (DMEM) (ATCC, VA, USA) containing 10% fetal bovine serum (FBS) (Atlanta Biologicals, GA, USA) and antibiotics,100 U/ml penicillin and 100 µg/ml streptomycin (Mediatech, VA, USA), at 37°C in a humidified 5% CO_2 incubator.

Cell Tagging: In order to visualize and image cells, MDA-MB 231 cells were tagged with the fluorescent tag, 5-chloromethylfluorescein diacetate (Cell Tracker Green CMFDA Dye) (Life Technologies, NY, USA). A working concentration of 5µM in serum-free media was used according to the instructions of the manufacturer.

Cell Treatments: Cells below 80% confluence were serum starved overnight in DMEM media containing no FBS. For drug treatment experiments, cells were treated with a sphingosine kinase inhibitor (SKI) compound which is known to exhibit antitumor activity [46, 47]. In order to do so, cells were incubated with the commercially available SKI compound, 5-(2-Naphthalenyl)-1H-pyrazole-3-carboxylic acid 2-[(2-hydroxy-1-naphthalenyl) methylene]hydrazide (SKI-I, ab142209) (Abcam, MA, USA). SKI-I was dissolved in dimethyl sulfoxide (DMSO) (Life Technologies, NY, USA) to make stock solutions. Aliquots were stored at -20°C for further use. SKI-I stock solution was diluted in growth medium to a final concentration of 5µM for cell treatment. Cells were incubated with the drug solution 24 hours prior to experiments and serum starved overnight.

II. Cell seeding of devices

In order to seed cells, devices were sterilized by 70% ethanol and exposed to UV overnight. Cells were harvested, suspended in serum-free media and passed through a cell strainer, Partec CellTricks (Sysmex, IL, USA), to remove cell aggregates and obtain single cell suspensions. Three separate experiments were performed; migration of serum-starved control cells towards media without serum (-FBS), media with serum (+FBS), and serum-starved SKI-I treated cells towards media with serum (SKI-I + FBS). Based on the corresponding experiment, growth medium

containing no or 10% FBS was loaded into the bottom chamber of the device as a chemoattractant for serum starved cells. The cells (50,000 cells/ 200µl) in serum-free media were introduced on top of the membrane and devices were incubated at 37°C in a humidified 5% CO_2 incubator.

III. ***Cell viability assay***

At the end of each experiment, a viability assay was performed by tagging dead cells on top of the membrane using Ethidium Homodimer-1 (EthD-1) (component B in Live/Dead viability kit for mammalian cells) (Life Technologies, NY, USA) at a final concentration of 2µM. Fluorescent images were acquired using a Zeiss Axio Imager (Germany). For each device, a representative field of view was imaged and live (green cells previously tagged with CMFDA tag) and dead cells (red) were counted using the free public domain image processing software, ImageJ (http://imagej.nih.gov/ij/). Viability for –FBS, +FBS, and SKI-I+ FBS experiments were measured at 87.69± 2.65, 89.98± 2.76, and 83.67± 2.36 respectively.

IV. ***Image acquisition and analysis***

Cell migration was observed by imaging the bottom side of the porous silicon membrane using a Zeiss Axio Observer.Z1 inverted epifluorescence microscope (Germany) with a 20× objective lens and imaged using a Zeiss AxioCam MRc camera (Germany). In order to obtain an overall image of the membrane, 154 frames were obtained and stitched together using the stitching utility of the Zen software. Images were acquired at 2, 6, and 12 hour time points.

ImageJ was used to analyze the acquired images. Initially a background subtract function was implemented on the images to even out the background. Afterwards images were converted to binary format using the color threshold tool in ImageJ. The particle analyze tool was used to create final masks for cell migration quantification. Artifacts and showing pores which did not contribute to the actual cell migration were removed by adjusting a size threshold of 80–110 pixels in the particle analyze tool. This threshold was determined for each experiment based on comparison with the original fluorescent image. The migration of cells in each condition was reported based on the total pixel area of the dark spots.

2.3 Results

I. Fabrication

The fabrication process flow includes the steps to fabricate the microchannel on the back and the pores on the front of a double-side polished 300 (±5) µm-thick silicon wafer as shown in Figure 5-1. The pore parameters on a high resolution chrome mask (The Photoplot Store, Co) with (r=8µm and d=50) was designed and used for lithography. In order to fabricate the pores, first, SPR 220.3 (MicroChem, MA, USA) photoresist is patterned, exposed with vacuum contact, and developed on the silicon wafer. The pores are etched using the recipe shown in Table 5-1 by an Alcatel AMS-100 DRIE (France) (Figure 2-1a). The pores are etched ~5µm more than the desired membrane thickness to ensure that they are through when the backside channel is etched. Next, a 400nm-thick silicon oxide layer is deposited utilizing a PECVD (Orion, AZ, USA) (Figure 5-1b). This oxide layer serves as a protection layer when the back-side etching of the channel meets the etched pores. It also enables the PDMS bonding to the device by activating the O_2 groups and enhances the cell attachment to the surface by making it hydrophilic. Then, the thickness of the silicon wafer is measure utilizing a Bruker DektakXT (MA, USA). This measurement is done at this stage to minimize the contamination of silicon wafer prior to the pore fabrication. Next, the wafer is cleaned thoroughly by oxygen plasma cleaning (Trion RIE, AZ, USA) and immersing in a Nanostrip (Cyanteck, CA, USA) solution, rinsed with di-ionized (DI) water, and dried at 150^{o}C for 15 mins. Next, the microfluidic channel with a central well is fabricated on the back-side of the silicon wafer utilizing the back-side alignment and DRIE etching. The central square well and microfluidic channel are 4mm and 1mm-wide, respectively. In order to fabricate the mask, AZ9260 (AZ Electronic Materials, NJ, USA) photoresist is patented, aligned, exposed and developed. The silicon from the pore side is spun with SPR220.3 photoresist and glued to a clean silicon wafer. The second silicon wafer seals the DRIE substrate and contains the back-side cooling He gas once the pores are exposed during the channel etching.

Table 2-1 The DRIE etching parameters.

DRIE Uniform Etch Parameters		LF Pulse Generator Parameters		Gas Parameters	
ICP power	**1800 W**	**H power**	**100 W**	**SF_6 flow rate**	**300 sccm**
Chamber pressure	**$3.5e^{-2}$ mbar**	**H time**	**20 msec**	**SF_6 time**	**6 sec**
Temperature	**0°C**	**L power**	**0 W**	**C_4F_8 flow rate**	**150 sccm**
He pressure	**10 mbar**	**L time**	**80 msec**	**C_4F_8 time**	**2 sec**

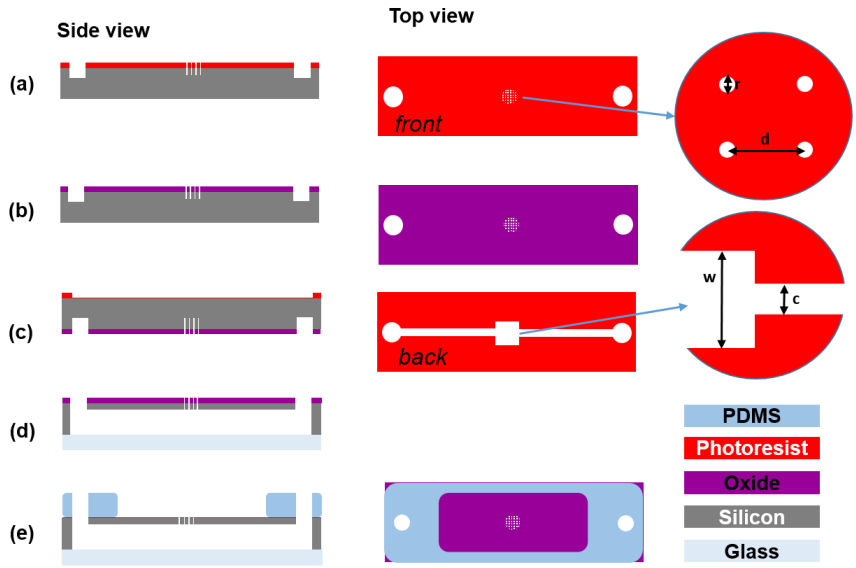

Figure 2-1 The side and top view of the fabrication process flow of deep channel and though-silicon via etching (a) Pattering photoresiste and DRIE etching of pores, (b) stripping PR and depositing the oxide layer, (c) back-side alignment and lithography of microchannels, (d) back-side channel DRIE etching and glass seal, and (e) PDMS well bonding.

The microfluidic channels are etched using the DRIE utilizing the same recipe provided in Table 2-1. The etch rate was carefully measured at different etch points to obtain a 30µm-thick membrane (wafers etched for ~270µm). The glued wafers are immersed in a warm PRS2000 solution for 10 mins until they are detached. The devices were then cleaned (O_2 plasma and

Nanostrip) and anodically bonded to a 500µm-thick Borofloat 33 glass wafer utilizing a Karl-Suss SB6 bonder (Germany) to seal the microfluidic channels. They are then diced and each individual device is O_2 plasma-bonded utilizing a Harrick Plasma cleaner (NY, USA) to a thick PDMS with the mixture ratio of 10:1 Sylgard 184 (Dow Corning, MI, USA). Figure 2-2 shows the image of the bonded devices and ESEM images of the pores.

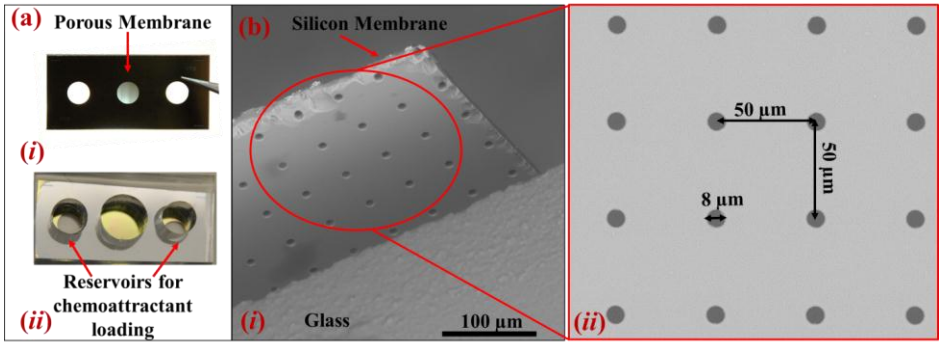

Figure 2-2 (a)(i) Final fabricated device before bonding to PDMS, (ii) final device after bonding to PDMS well, (b) (*i*) ESEM image of the overall device, (*ii*) close up image of the pores.

II. Experiments

In order to verify the performance of the fabricated platform, experiments were performed as mentioned in the methods section. Figure 2-2a shows images acquired from the underside of the membrane for the different experiments at 2, 6, and 12hour time points. Migration for each experiment is reported based on the total pixel area as mentioned in the methods section (Figure 2-2b). The final counts are shown in Figure 2-2c.

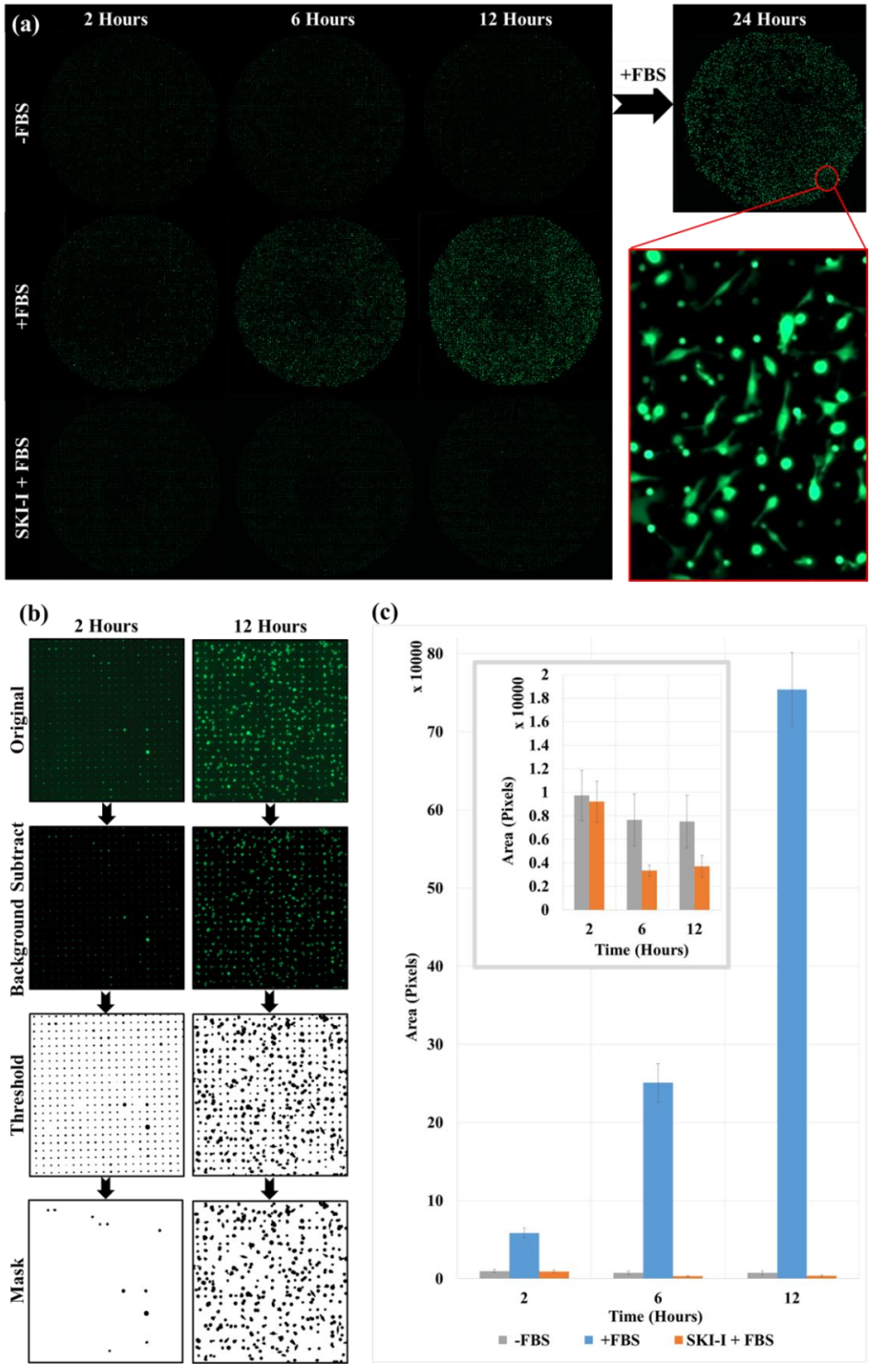

Figure 2-3 (a) Overall image of the migration membrane in –FBS (top), +FBS (middle) and SKI-I+ FBS (bottom) experiments, (b) An example of the image analysis procedure for a +FBS experiment at 2 (left) and 12 hours (right), (c) migration profile of experiments at 2,6, and 12 hour time points for 5 independent experiments represented as mean ±SEM.

Random movement and migration of the cells in the absence of a chemical gradient was studied by creating a serum-free environment above and below the membrane (-FBS experiment). Cells showed low migration after 12 hours since there was no serum available to activate a migration response in the cells. However, replacing the serum-free media below the membrane with media containing 10% FBS at the 12 hour time point and inspecting the membrane 12 hours after this change, it was evident that many cells had migrated and attached to the underside of the membrane. This phenomenon demonstrates the effective creation of a chemical gradient across the membrane and the ability of MDA-MB 231 cells to migrate through this membrane in the presence of such a gradient. Moreover, the random migration of cells which may interfere with the actual migration response caused by a chemoattractant is low in this platform. Hence further experiments were carried out to verify the function of this device to distinguish the migration behavior between normal and drug treated cells

Migration of the untreated cells in the presence of a serum gradient (+FBS experiment) was low at the 2 hour time point (Figure 2-3a). As time progressed, a clear distinction and migration was observed at the 6 hour time point and by the 12th hour the migration and attachment of cells to the underside of the silicon membrane was evident as shown in Figure 2-3a. In contrast, migration of the SKI-I treated cells showed no progress even after 12 hours. This can be an indication that the drug has affected the cells, limiting their motility and migration and making it impossible for them to get into the pores and move to the other side of the silicon membrane. Based on this observation, the fabricated device can be used to monitor and distinguish between drug treated and non-treated cells.

2.4 Discussion

Cell migration plays a key role in biological processes such as embryonic development, immune response, would healing, angiogenesis and cancer metastasis. Evaluation of the migration behavior of cells in a controlled environment is of interest to researchers as it can expand our knowledge of the signaling pathways involved in these events and the modulation of chemotactic response of cells by pharmaceutical agents. Commercially available Boyden chambers provide end point analysis of cell migration via a one-time use polycarbonate membrane housed inside a culture plate which needs to be post-processed (i.e. Fixing and staining) to provide final results.

The fabricated micro-Boyden chamber migration assay in this work is composed of a porous silicon membrane and microfluidic channels on a single silicon substrate bonded to a glass enclosing which enables real-time analysis of cell migration using a microscope. Moreover, no post processing of the silicon membrane is needed; it can be cleaned at the end of each experiment and reused in contrast to the one-time use polycarbonate membranes. Using a silicon substrate, one can take advantage of readily available fabrication methods in the semiconductor industry to upscale the production of this platform. Taking advantage of these fabrication techniques, it is also possible to create different pore sizes and pore densities on a single membrane whereas such an option is not available in the conventional Boyden chamber assay.

This work furthermore utilizes DRIE to fabricate a deep microfluidics-enabled micro-channels with porous thin membrane on a single silicon wafer with control on the membrane thickness. Since deep etching of the back-side of the microchannel defines the thickness of the membrane, it is vital to achieve a uniform etch profile in order to fabricate the membrane with minimal thickness variation across the area that encloses the pores. Non-uniform etching will result in faster etching of the channel area than the well area which will leave the channel area thinner. If this is not checked, it might result in complete removal of the channel when etching to reduce the membrane thickness. Furthermore, a non-uniform etch profile will inadvertently produce a high level of variation on the membrane thickness across the wafer resulting in fewer usable devices. Typically, increasing the etch rate alleviates the non-uniform etching problem. We explored the effect of several parameters that affect the etch uniformity across the devices and the wafer. Reducing SF_6 etch time from 6 secs to below 4 secs in the time-multiplexed DRIE etch recipe, dramatically reduces the etch uniformity. It caused a severe reduction in etch rate on the device, especially on the outer side of the wafer. In such cases, some of the devices at the center of the wafer were etched and met the desired membrane thickness requirement, while the pores on devices at the corners were not yet visible from the channel on the back-side. The reduced etch rate also caused a non-uniform membrane with a groove-shaped pattern. The inductively coupled plasma (ICP) power, low frequency (LF) power, and temperature may also be adjusted to increase the etch rate and improve uniformity. Since the wafer is glued to a dummy wafer, temperature was not elevated and kept at $0^{o}C$ as the photoresist glue is not a good heat conductor and increased temperature might damage the contact between the two wafers. Excessive etch rate during the final phase of the etching (last 10µm) is also avoided to precisely determine the membrane thickness.

SKIs are a class of drugs with anti-tumor therapeutic potential due to their ability to inhibit tumor growth by intercepting the sphingosine kinase pathway [46]. They have been shown to have anti-proliferative effect on a variety of tumor cell lines including breast cancer cells [47]. We used the drug SKI-I to treat a highly metastatic cell line, MDA-MB-231, and used this as a model to test the working-principle of our microfluidic migration assay. Our results confirm that SKI-I causes MDA-MB-231 breast cancer cells to become apoptotic and greatly diminishes their migration through the pores in the silicon membrane. Hence, this assay is suitable for evaluating the effect of pharmaceutics and other stimuli on the migration behavior of cells.

The developed platform lends itself to the incorporation of improvements that will expand its functionality. For instance, a biocompatible hydrogel can be introduced into the top chamber to create a physiologically relevant model for cell invasion. The introduction of chemicals such as VEGF into the bottom channel can be used to create an *in vitro* model for angiogenesis. The addition of electrodes on the bottom side of the membrane, will enable automated label-free measurements of cell migration. The integration of the micro-channels with porous membrane also can be used to improve microfluidic circulation and create gradient profiles across the membrane. Further, the employment of multiple stages of such blocks can result in high throughput cell migration screening based on different candidate-drug treatment plans.

2.5 Conclusion

In this work we have presented the fabrication of a silicon-based device for cell migration analysis as an alternative to conventional Boyden chamber assays. This platform integrates a porous membrane with a chemoattractant reservoir and microchannels in a single silicon wafer, reducing the number of components in a conventional Boyden chamber assay. Characterization and optimization of the microfabrication techniques with a focus on the optimization of the deep reactive ion etch parameters are presented to create porous silicon membranes with minimum thickness variance across a single membrane and between different membranes on a wafer, while controlling the pore etch rate and avoiding under/over-etching of the pores.

The experimental results we obtained from this device demonstrate its capability to detect migration towards serum in MDA-MB 231 cells. This functionality is emphasized by the fact that the cells exhibit very low migration towards serum-free media, whereas when serum is added to

the same media, cells migrate to the underside of the membrane after 12 hours of no migratory activity. Moreover, the migration of drug treated cells was studied using this device. SKI-I treated cells showed very low -close to zero- migration towards serum on this platform, exhibiting the future potential of this device to survey other potential drug treatment plans.

Chapter 3. Dielectrophoresis –based Differentiation of Cells

3.1 Introduction

Biophysical markers of the cell such as their dielectrophertic signature can prove a beneficial tool to differentiate between live/dead cells [48], separating circulating tumors cells from blood samples [49], and to understand the mechanisms underlying cancer and drug sensitivity [50]. This work presents a novel method to distinguish between various established cell lines through their dielectrohoretic response. In addition, the response of a hormone-responsive breast cancer cell line model to anti-tumor drug stimuli is explored through the use of a dielectrophoresis (DEP)-based method.

The proposed method in this work differs greatly from traditional DEP characterization methods as it involves the use of insulator-based DEP (iDEP) rather than electrode-based DEP. Moreover, the electrodes used in this study are designed to be off-chip, minimizing any contact between the sample and electrodes. This method referred to as the off-chip passivated-electrode and insulator-based DEP microchips (OπDEP) has been demonstrated to distinguish between live/dead bacteria [51].

LCC1 and LCC9 cells are hormone-receptor positive cells which are derived from MCF-7 cells. LCC1 cells are selected from MCF-7 cells *in vivo* and are estrogen independent and anti-estrogen sensitive. LCC9 cells are selected *in vitro* from LCC1 cells and are estrogen independent and anti-estrogen resistant. Based on these characteristic, each cell type exhibits a different behavior in response to cancer treatment drugs. For example, the anti-tumor drug GX15-070 (obatoclax) has been shown to be more effective in reducing the cell density of anti-estrogen resistant cells (LCC9) compared to anti-estrogen sensitive cells (LCC1) [52]. In this work we characterize and distinguish between multiple breast cancer cell lines using OπDEP platform, while assessing the drug sensitivity of select cells (LCC and LCC9) using specific drug stimuli.

3.2 Methods

I. Device Fabrication

Fabrication process of the OπDEP device has been mentioned in detail in previous work [51]. In short photolithography, deposition of chrome and gold, and a lift-off process were employed to

create a pair of electrodes with dimensions of 1000 and 600µm in width and horizontal spacing respectively on a 500µm thick pyrex wafer. Polydimethlsiloxanne (PDMS) (Ellsworth Adhesives, WI, USA) microfluidic channels with insulator posts (100µm in diameter with 50µm spacing) were fabricated using mold replication and a dry etched silicon wafer as the master. Inlet and outlets were created on each device and the device was bonded to a 100µm thick #0 cover glass slide (Electron Microscopy Sciences, PA, USA) which separates the channel from the electrodes. The final device set up is shown in Figure 1a.

II. Cell Culture and Treatments

LCC1 and LCC9 cell lines were provided by Dr. Ayesha Shajahan-Haq (Lombardi Cancer Center, Georgetown University, Washington, DC). MDA-MB-231 and MCF-7 cells were obtained from American Type Culture Collection (ATCC, VA, USA). Cells were maintained in T-25 flasks in Minimum Essential Medium (MEM Richter's modification) (Life Technologies, NY, USA) containing 5% Donor Calf Serum Charcoal Stripped (Valley Biomedicals, VA, USA) and antibiotics, 100 U/mL penicillin and 100µg/mL streptomycin (Mediatech, VA, USA), at 37°C in a humidified 5% CO2 incubator.

In order to analyze drug sensitivity, LCC1 and LCC9 cells were treated GX drug at a non-lethal dose (500nM) for 12 hours. Stock solutions of Obatoclax Mesylate (GX15-070) (Selleckchem, TX, USA) was prepared in dimethyl sulfoxide (DMSO) (Life Technologies, NY, USA), stored at -80°C for future use, and diluted in culture media to the desired concentration for each experiment.

After the desired treatment, cells were harvested and tagged with the fluorescent tag, 5-chloromethylfluorescein diacetate (Cell Tracker Green CMFDA Dye) (Life Technologies, NY, USA) with a working concentration of 5µM in the low conductivity DEP buffer. The DEP buffer was prepared (8.5g sucrose and 0.725mL MEM in 100mL DI water) with a measured conductivity of 113 µS/cm. Additional wash steps were employed to clear the cell solution from residual drug or tag which may vary the solution conductivity. Trypan blue (Sigma-Aldrich, MO, USA) assay was employed after the preparation steps and before each run to verify the viability of the sample.

III. Experimental Setup

Prior to DEP trials, PDMS devices were placed under vacuum for at least 30 minutes. Posts on the device were properly aligned such that the posts were directly above and between the two

electrodes as indicated in Figure 3-1. A 1mL syringe containing fluorescently tagged cell solution was then connected to the device via tubing and the solution was driven through the channel at a constant flow rate using a Pump11 Elite (Harvard Apparatus, MA, USA) syringe pump. Voltages at different frequencies in the frequency range of 50kHz up to 1MHz were applied for 20 seconds to the electrodes using a 50MHz Function Generator (B&K Precision, CA, USA) and Voltage Amplifier (FLC Electronics AB, Sweden) to initiate trapping of the cells. Trapping of the cells was observed using a Zeiss Axio Observer.Z1 inverted epifluorescence microscope (Germany) with a 10X objective lens and imaged using a Zeiss AxioCam MRc camera (Germany). Finally, trapping efficiencies are calculated as a ratio of trapped cells to total cells in each run.

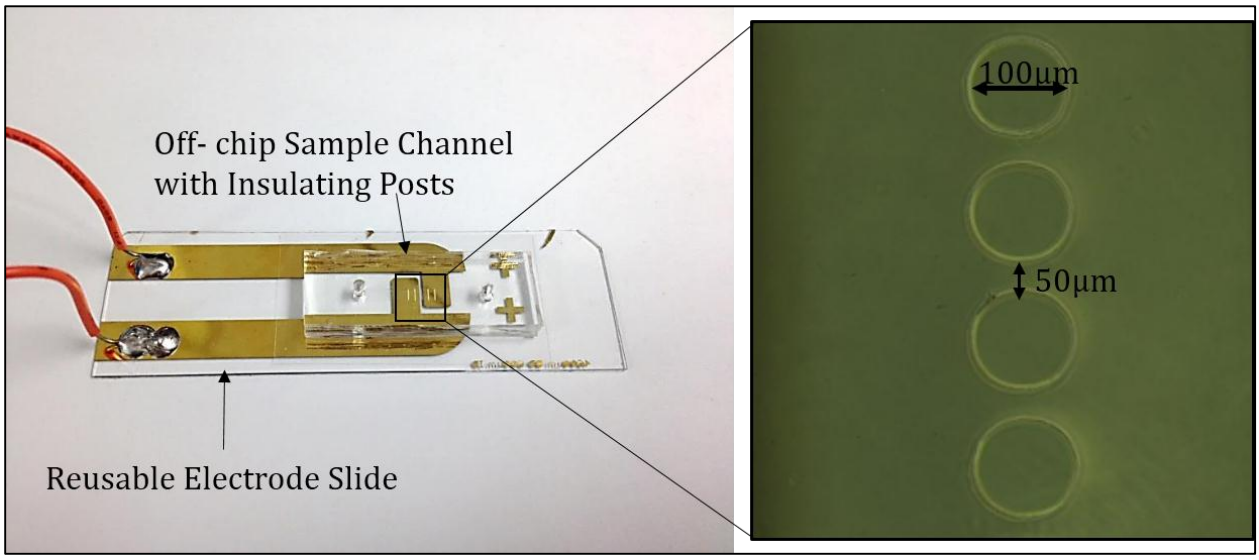

Figure 3-1 Experimental setup of the device, the PDMS channel bonded to a thin glass is placed on top of the electrodes. Inset shows the PDMS insulating posts along the channel.

IV. SEM Sample Preparation

Cells were grown and drug treated on individual glass slides and fixed using a 4% formaldehyde solution (Baker, PA, USA). Samples were post-fixed in 1% Osmium Tetraoxide, dehydrated in graded ethanol series (15%, 30%, 50%, 70%, 95%, 100%), and critical point dried. After sputter coating the samples with gold, SEM images were acquired using a Carl Zeiss EVO 40 SEM (Germany).

V. Cell Size Measurement

For each case, the size of the cells in the suspensions were measured by capturing images using the epifluorescence microscope and analyzed by image processing software, Zen Pro Blue. 50 cell sizes were measured for each case and the final cell size was reported as the mean ± SD.

3.3 Results & Discussion

I. Optimization of Experiment Variables

In order to get accurate and comparable results between the two cell lines, various parameters for the experiments were optimized. The two main parameters in the OπDEP platform are the flow rate of the sample solution and the voltage applied to the off-chip electrodes. The flow rate is a significant factor since trapping in the channel is the result of the interplay between the dielectrophoresis force and the drag force [51]. Three representative flow rates,10, 20, 50$\mu L.hr^{-1}$, were tested on LCC1 and LCC9 untreated samples (data not shown). The optimum flow rate was determined to be 20$\mu L.hr^{-1}$, since 10$\mu L.hr^{-1}$ was too low to keep a consistent flow and 50$\mu L.hr^{-1}$ was too high to observe trapping in the working frequency and voltage range of the voltage generator/amplifier system. Thereafter, three representative voltages 60, 80, 160 Vpp, were applied to find the optimal applied voltage (Figure 3-2). 80Vpp was found to be the best option since it was high enough to observe trapping in the working frequency range (50-1000 kHz) for the LCC1 cell line, but not too high to lose sensitivity and not distinguish effectively between the two different cell lines.

Using the optimal flow rate and applied voltage, cells were characterized and different trapping profiles were observed. Moreover, two independent runs using a different cell solution and also a different device were carried out using LCC1 cells to assure the reliability and repeatability of the experiments (data not shown).

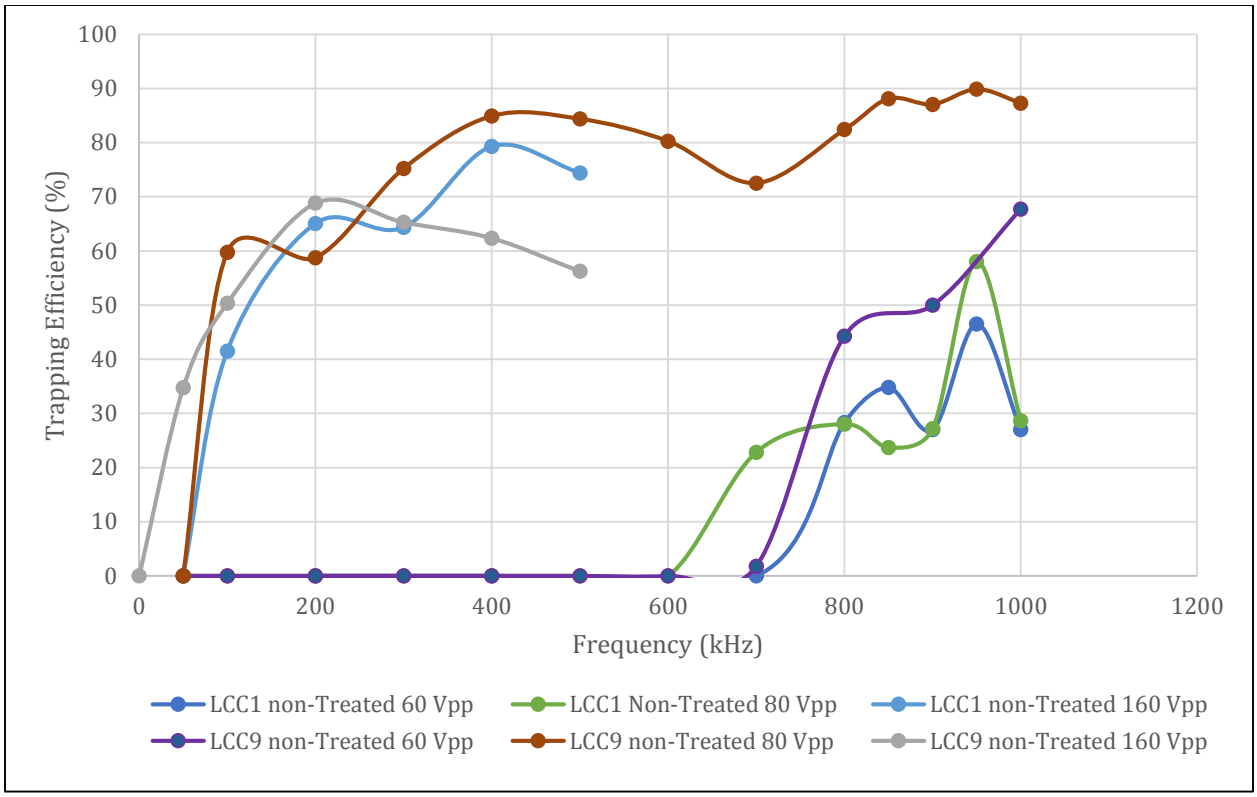

Figure 3-2 Trapping efficiency profile of non-treated LCC1 and LCC9 cells at various applied voltages.

II. Differentiation Among Different Cell Lines

Trapping profile of the different cell lines revealed distinct trapping profiles for each as shown in Figure 3-3. Based on the results, LCC9 cells have the lowest crossover frequency and highest relative trapping efficiency. Careful inspection of the trapping response reveals that the overall LCC9 and MDA-MB-231 cells profiles are similar to each other, while LCC1 more closely resembles the parent cell, MCF-7. Various reasons can be attributed to these differences such as cell size and electrical properties of the cell. One interesting explanation may relate the aggression characteristic of these cells, MDA-MB-231 and LCC9 cells are more aggressive type pf cancer, while LCC1 is not at aggressive and more similar to MCF-7 cells.

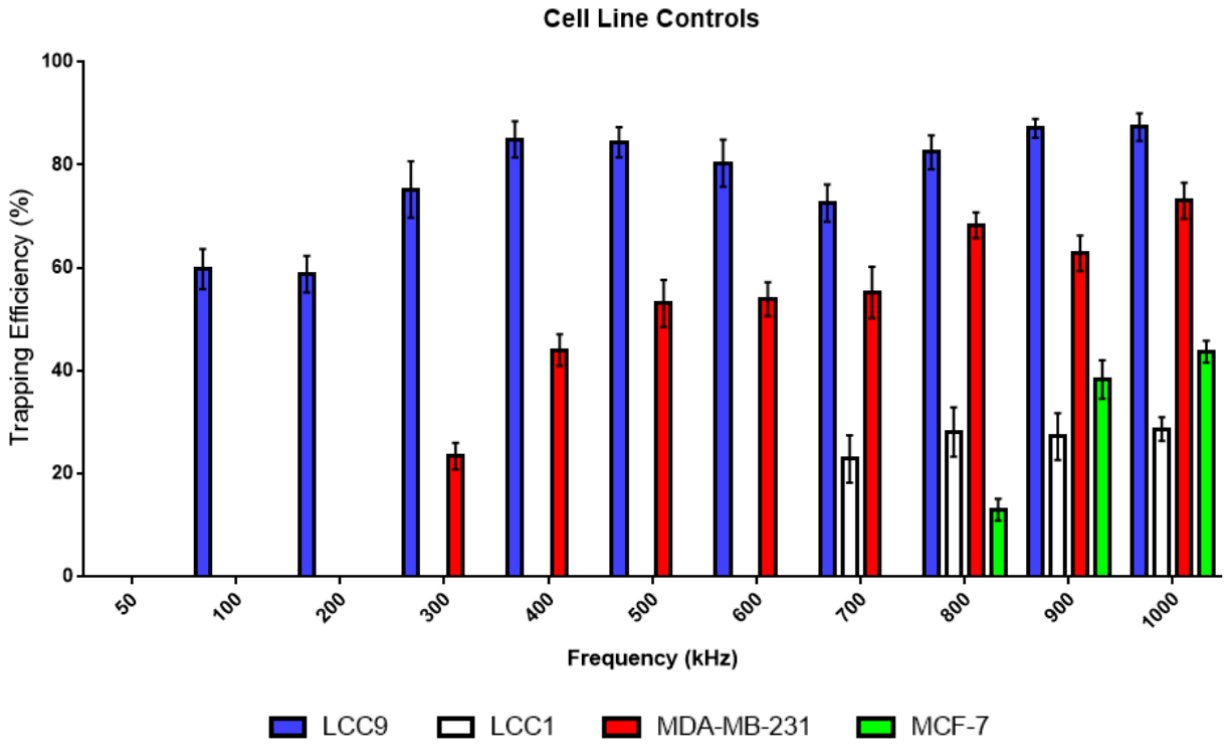

Figure 3-3 Trapping profile of different cell lines, each bar represents mean ± SEM for at least 3 experiments (n>=3).

III. Characterizing Drug Response using DEP

Figure 3-4 shows the response of LCC cell to GX treatment. Based on these results, treated and untreated cells in both cases have distinguishable profile. In both, the cross over frequency shifts to a higher value which can be indicative of a change in the cell size and/or changes in the properties of the cell which relate to the electrical properties of the cell.

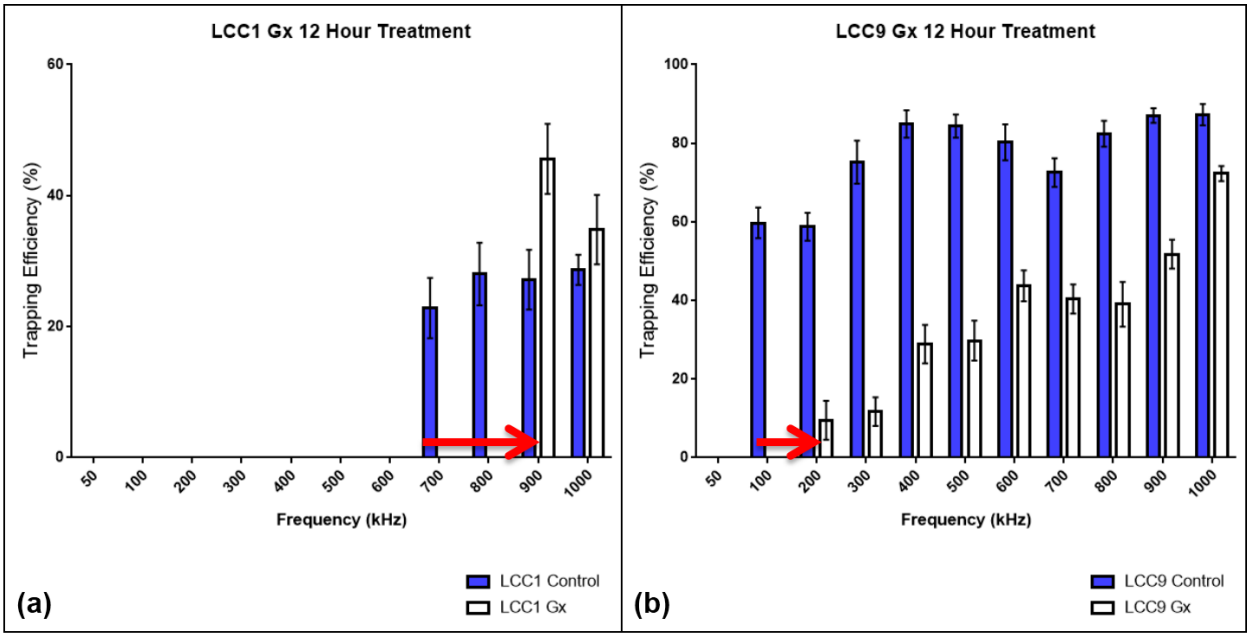

Figure 3-4 Trapping profile of control (untreated) and GX treated (a) LCC1 and (b) LCC9 cells, each bar represents mean ± SEM for at least 3 experiments (n>=3).

IV. Morphology of Untreated and GX-treated LCC Cells

SEM images of the treated and untreated LCC1 and LCC9 cell reveals changes in the cell membrane (Figure 3-5). In LCC1 cells, once smooth surfaces become very ruffles with many protrusions appearing on the surface. In contrast LCC9 cells have a very rough surface in the beginning, but after undergoing treatment they lose many of these features and become smoother. In general, smoother surfaces are associated with lower membrane capacitance, leading to a higher cross over frequency [53]. However, one cannot simply rely on the membrane morphology to estimate the changes in cell capacitance, since capacitance is a factor of various factors such as the area, thickness, and permittivity of the membrane. The membrane morphology can hint changes on the surface area change, but other parameters need more detailed investigation to observes the undergoing changes. Considering constant membrane permittivity and thickness, our findings regarding LCC9 confirm that the smoother membrane contributes to a higher cross over frequency which may be due to the capacitance and surface area change. In contrast, this hypothesis is not confirmed in LCC1 cells, which leads to the assumption that a more significant mechanism is happening in these cells and/or influencing the membrane thickness, membrane permittivity, or cytoplasm or a combination of these parameters. Significant changes in the cytoplasm behavior has been previously shown in other

studies [50]. In order to pinpoint the exact mechanism further detailed investigation on the suggested parameters is needed.

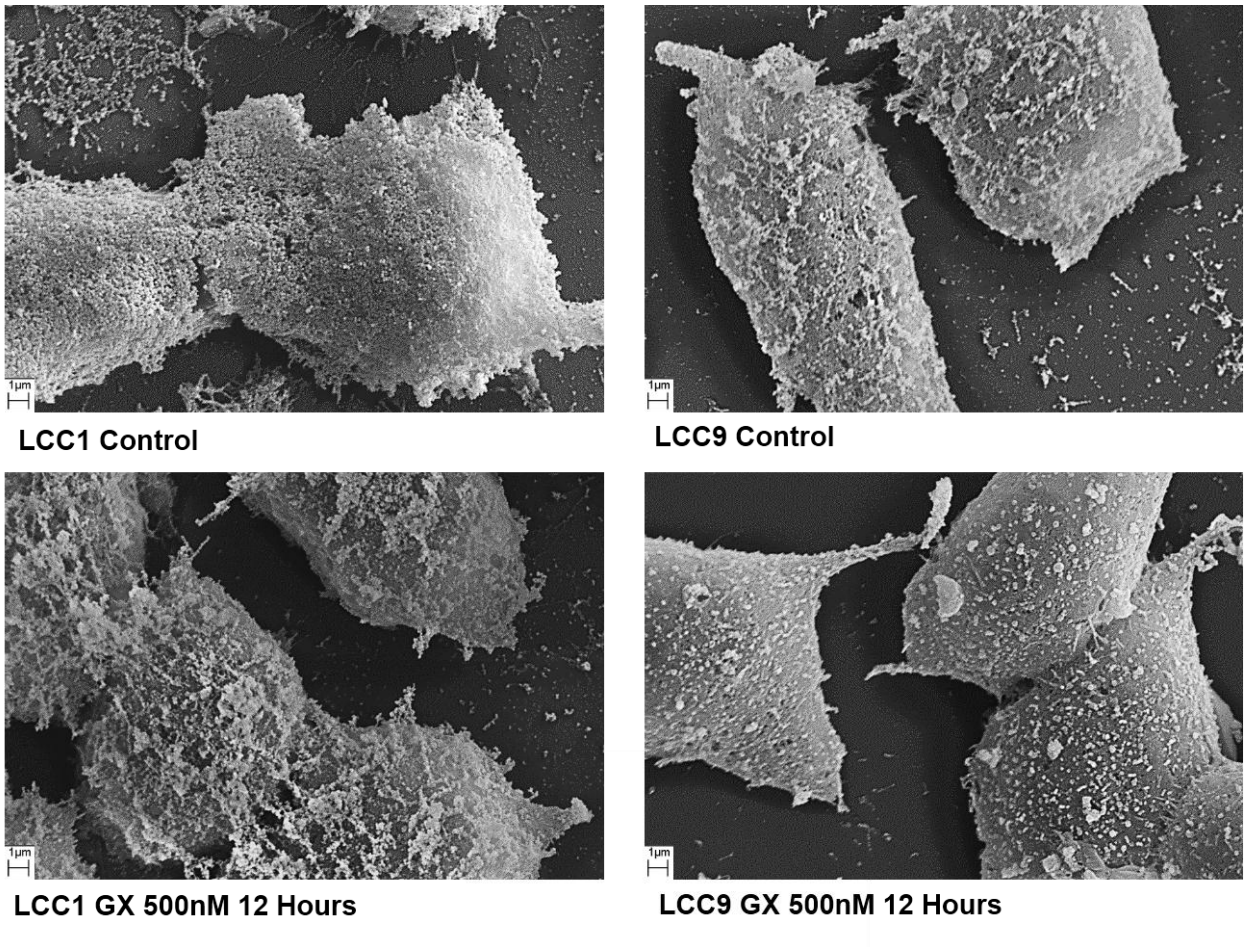

Figure 3-5 SEM images of control and GX treated LCC1 and LCC9 cells.

V. Measured Cell Sizes

Measured cell sizes are reported in Table 1. LCC9 treated cells show a significant decrease in cell size, while LCC1 cells are slightly smaller than the untreated cells. The cross over frequency observed in the tapping profile is inversely related to the size of the particle. Therefore, a decrease in cell size will result in an increase in the crossover frequency. This phenomenon is observed in LCC9 cells. However, LCC1 cells exhibit a different trend, which enhances the probability of another mechanism contributing to the trapping response. As mentioned in the previous section, one such effect can be caused by how the cytoplasm is being changed during treatment, and the change being so significant that it changes the lower frequency DEP response.

Table 3-1 Measured cell size for untreated and GX treated LCC1 and LCC9 cells.

Treatment	LCC1 (μm)	LCC9 (μm)
Control	13.06+/- 1.94	14.75 +/- 1.25
GX 500nM 12 Hours	14.62 +/- 1.43	10.56 +/-1.37

3.4 Conclusion

Utilizing the previously established OπDEP platform, we have shown that different cell lines exhibit different and distinctive trapping profiles with differing trapping onset frequency. Moreover, when the cells are exposed to a chemical stimulus, the initial trapping frequency and the trapping efficiencies vary and the treated cells are clearly differentiated from non-treated cells, exhibiting the applicability of this method for drug sensitivity studies. These profiles can be correlated and fitted to equivalent electrical models to fully understand the effect of the drug. Further research needs to be performed to find the link between the DEP characteristics and the biological phenomenon which lead to each kind of profile.

Chapter 4. Dielectrophoresis as a Cell Characterization and Drug Assessment Tool

4.1 Introduction

Breast cancer is the leading cause of cancer related death among women aged 20 to 59 years old in the United States [2] and the second leading cause of cancer related deaths among women of all ages, affecting 1.7 million women each year [3]. It is estimated that breast cancer alone will account for 29% of all new cancer diagnosis in 2016 [2]. Breast cancer is unique in the sense that it includes various types of resistance behavior, leading to different clinical treatments and outcomes [4]. Breast cancer is generally categorized in three major types based on immunohistochemical properties: 1) hormone receptor (HR)-positive for estrogen (ER) and progesterone (PR) hormones, 2) human epidermal growth factor receptor 2 positive ($HER\text{-}2^{+}$) and, 3) triple-negative breast cancer (TNBC) [3]. HR^{+} type accounts for approximately 85% of all breast cancers and has the best prognosis among all types. Endocrine therapies such as tamoxifen and aromatase inhibitors (AI) are used for treatment of this type. Approximately 15% of breast cancer are TNBC type which does not over express hormone receptor, therefore rendering targeted hormonal therapies useless and having the worst prognosis [3]. Although the majority of diagnosed cases are HR^{+} which exhibit a high treatment success rate, one cannot evade the possibility of inherent or acquired resistance of the cancer to hormone therapies [52]. Thus, improving diagnostic methods which can detect such resistance deem necessary to further enhance the survival rates of breast cancer recurrence or acquired resistance cases.

Biophysical markers of the cell such as its dielectrophertic signature can be a beneficial tool to understand the mechanisms underlying cancer and drug sensitivity. Dielectrophoresis (DEP) is an electrokinetic-based technique in which uncharged particles in suspended in a fluid can be moved via polarization forces induced by an inhomogeneous electric field [33]. DEP is a highly versatile and customizable method which can be used to manipulate bioparticles based on their dielectric properties [34]. Separation and enrichment of bacterial samples [54-56], the study of drug induced apoptosis of cancer cells [48, 57, 58], detection and separation of circulating tumor cells from blood samples [49], and separation of stem cells from somatic cells [59] are just a few examples

of the application of DEP based methods for characterization and manipulation of biological samples. While the main goal of most DEP based microfluidic devices is aimed at sorting and sample enrichment, the dielectrophoretic response over a frequency range of applied electric field can be a valuable characterization tool since it contains information not only on cell size but also the intrinsic electrical properties of the cell [60].

Traditionally, electrodes in direct contact to the biological samples were used to induce a DEP response in samples. However, such methods pose limitations such as sample contamination, electrolysis, and delamination of electrodes [61]. In recent years an alternate method, referred to as insulator-based DEP (iDEP), has been explored in which non-uniform electric fields are created using insulating structures in the device rather than the geometry of electrodes [62]. Moreover, electrodes can be placed in remote contact to the insulating posts to lower Joule heating in the devices and eliminate the possibility of sample contamination. This method, known as the off-chip passivated-electrode insulator-based dielectrophoresis (OπDEP), has been previously established in our lab for separation and enrichment of bacterial samples [51, 54]. In the OπDEP microfluidic chip, off-chip electrodes are used to capacitively couple the electric field into the channel with insulating structures, hence utilizing the iDEP concept, without the limitations of heating in the channel.

In this work we use the OπDEP platform as a powerful characterization tool to study the underlying mechanisms of drug resistance in HR^+ breast cancer cell lines. For this purpose, two estrogen-independent cell lines derived from the MCF7 cell line (ER^+, estrogen-dependent) are selected as models for this study. The selected cell lines represent drug resistance at different levels. MCF7/LCC1 are estrogen-independent but antiestrogen sensitive, while MCF7/LCC9 are estrogen-independent and resistant to the estrogen receptor down regulator, Faslodex (ICI 182, 780) [52]. We characterize the dielectrophoretic response of these cells to estrogen and to the anti-estrogen drug, ICI, in order to find unique properties corresponding to each represented state of drug resistance.

4.2 Methods

I. Device Fabrication

Fabrication process of the OπDEP device has been mentioned in detail in previous work [51]. In short photolithography, deposition of chrome and gold, and a lift-off process were employed to create a pair of electrodes with dimensions of 1000 and 600µm in width and horizontal spacing respectively on a 500µm thick pyrex wafer. Polydimethlsiloxanne (PDMS) (Ellsworth Adhesives, WI, USA) microfluidic channels with insulator posts (100µm in diameter with 50µm spacing) were fabricated using mold replication and a dry etched silicon wafer as the master. Inlet and outlets were created on each device and the device was bonded to a 100µm thick #0 cover glass slide (Electron Microscopy Sciences, PA, USA) which separates the channel from the electrodes. The final device set up is shown in Figure 1a.

II. Cell Culture and Treatments

LCC1 and LCC9 cell lines were provided by Dr. Ayesha Shajahan-Haq (Lombardi Cancer Center, Georgetown University, Washington, DC). Cells were maintained in T-25 flasks in Minimum Essential Medium (MEM Richter's modification) (Life Technologies, NY, USA) containing 5% Donor Calf Serum Charcoal Stripped (Valley Biomedicals, VA, USA) and antibiotics, 100 U/mL penicillin and 100µg/mL streptomycin (Mediatech, VA, USA), at 37°C in a humidified 5% CO2 incubator.

In order to analyze drug sensitivity, each target cell line was treated with either 0.02% ethanol (vehicle), ICI 500nM, or Estrogen 10nM for a predefined treatment time (12, 24, 48, or 72 hours). Stock solutions of the anti-estrogen drug ICI 182,780 (Tocris, UK) and estrogen (β-Estradiol) (Sigma-Aldrich, MO, USA), were prepared in ethanol (Sigma-Aldrich, MO, USA), stored at -20°C for future use and diluted in culture media to the desired concentration for each experiment.

After the desired treatment, cells were harvested and tagged with the fluorescent tag, 5-chloromethylfluorescein diacetate (Cell Tracker Green CMFDA Dye) (Life Technologies, NY, USA) with a working concentration of 5µM in the low conductivity DEP buffer. The DEP buffer was prepared (8.5g sucrose and 0.725mL MEM in 100mL DI water) with a measured conductivity of 113 µS/cm. Additional wash steps were employed to clear the cell solution from residual drug or tag which may vary the solution conductivity. Trypan blue (Sigma-Aldrich, MO, USA) assay was employed after the preparation steps and before each run to verify the viability of the sample.

III. Experimental Setup

Prior to DEP trials, PDMS devices were placed under vacuum for at least 30 minutes. Posts on the device were properly aligned such that the posts were directly above and between the two electrodes. A 1mL syringe containing fluorescently tagged cell solution was then connected to the device via tubing and the solution was driven through the channel at a flow constant rate by a Pump11 Elite (Harvard Apparatus, MA, USA) syringe pump. Voltage at different frequencies in the frequency range of 50kHz up to 1MHz was applied for 20 seconds to the electrodes using a 50MHz Function Generator (B&K Precision, CA, USA) and Voltage Amplifier (FLC Electronics AB, Sweden) to initiate trapping of the cells. Trapping of the cells was observed using a Zeiss Axio Observer.Z1 inverted epifluorescence microscope (Germany) with a 10X objective lens and imaged using a Zeiss AxioCam MRc camera (Germany). Finally, trapping efficiencies are calculated as a ratio of trapped cells to total cells in each run.

IV. SEM Sample Preparation

Cells were grown and drug treated on individual glass slides and fixed using a 4% formaldehyde solution (Baker, PA, USA). Samples were post-fixed in 1% Osmium Tetraoxide, dehydrated in graded ethanol series (15%, 30%, 50%, 70%, 95%, 100%), and critical point dried. After sputter coating the samples with gold, SEM images were acquired using a Carl Zeiss EVO 40 SEM (Germany).

V. Cell Size Measurement

For each 72hour treatment, the size of the cells in the suspensions were measured by capturing images using the epifluorescence microscope and analyzed by image processing software, Zen Pro Blue. 50 cell sizes were measured for each case and the final cell size was reported as the mean ± SD.

4.3 Results

I. Optimization of DEP Experiment Variables and Repeatability of Runs

In order to get accurate and comparable results between the two cell lines, various parameters for the experiments were optimized. The two main parameters in the OπDEP platform are the flow rate of the sample solution and the voltage applied to the off-chip electrodes. The flow rate is a

significant factor since trapping in the channel is the result of the interplay between the dielectrophoresis force and the drag force [51]. Three representative flow rates,10, 20, 50µL.hr^{-1}, were tested on LCC1 and LCC9 untreated samples (data not shown). The optimum flow rate was determined to be 20µL.hr^{-1}, since 10µL.hr^{-1} was too low to keep a consistent flow and 50µL.hr^{-1} was too high to observe trapping in the working frequency and voltage range of the voltage generator/amplifier system.

Thereafter, three representative voltages 60, 80, 160 Vpp, were applied to find the optimal applied voltage (as shown in the previous chapter). 80Vpp was found to be the best option since it was high enough to observe trapping in the working frequency range (50-1000 kHz) for the LCC1 cell line, but not too high to lose sensitivity and not distinguish effectively between the two different cell lines.

Using the optimal flow rate and applied voltage, untreated LCC1 and LCC9 cells were characterized and different trapping profiles was observed for the two cell lines. Moreover, two independent runs using a different cell solution and also a different device were carried out to assure the reliability and repeatability of the experiments. Based on the graph in Figure 4-1, the two runs are very similar and it is safe to assume that the OπDEP platform can provide reliable results.

To ensure the viability of the cell sample during the period of the experiment, viability of the LCC9 untreated cells were measure at various time points after preparation and are reported in **Table 1**. Based on these results, the samples have acceptable viability up to the 3 hours after preparation in DEP buffer and at room temperature. However, almost all the results reported in this work have been gathered from experiments lasting less than 1.5hours.

Table 4-1 Viability of LCC9 untreated cells at different times after preparation.

Time (Minutes)	15	30	60	120	180	240
Viability (%)	98.35± 0.32	98.76 ± 0.56	97.42 ± 0.86	93.09 ± 0.84	93.27 ± 0.97	81.54 ± 2.85

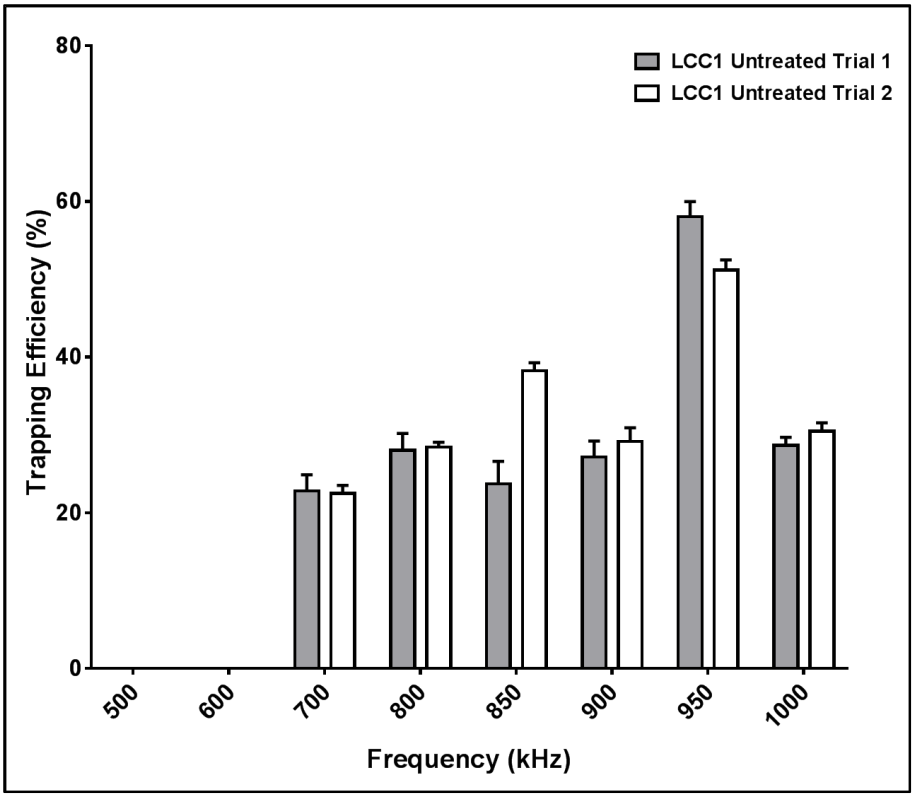

Figure 4-1 Trapping efficiencies for two independent runs of LCC1 untreated samples, each data point represents mean ± SEM for at least 3 runs (n>= 3).

II. Dielectrophoresis-based Characterization

Trapping efficiency graphs were created for the various experiment conditions as described in the methods section at 80 Vpp and 20µL.hr^{-1}. One representative graph for 48 hour treatments for each cell line is shown in Figure 4-2a, b. The main parameter of interest in these graphs is the frequency were the first trapping takes place, herein referred to as the **crossover frequency**. For the untreated cases, it was observed that LCC9 cells start trapping at 100kHz whereas this frequency for LCC1 cells is 700 kHz. This initial observation confirmed that these two cell lines exhibit different electrical properties. Moreover, the vehicle treatment did not alter the overall trapping profile compared to the untreated samples, showing that the vehicle does not change the cells in a significant manner. The main finding of the experiments have been summarized in Figure 4-2c, d.

In the case of LCC1 cells, ICI treatment caused the crossover frequency to decrease from 700kHz to 300kHz over the course of 72 hours, whereas estrogen treatment did not have a significant effect, with a frequency shift of only 100kHz after 72 hours of treatment. In contrast,

ICI and estrogen treatments caused the crossover frequency to increase from 100kHz to 700 and 800kHz respectively. Based on the results, the treatments do not have a significant effect on the trapping efficiency of LCC1 cells. For LCC9 cells, the trapping efficiency for the ICI treatment decreases slightly whereas a significant decrease is observed in estrogen treated samples.

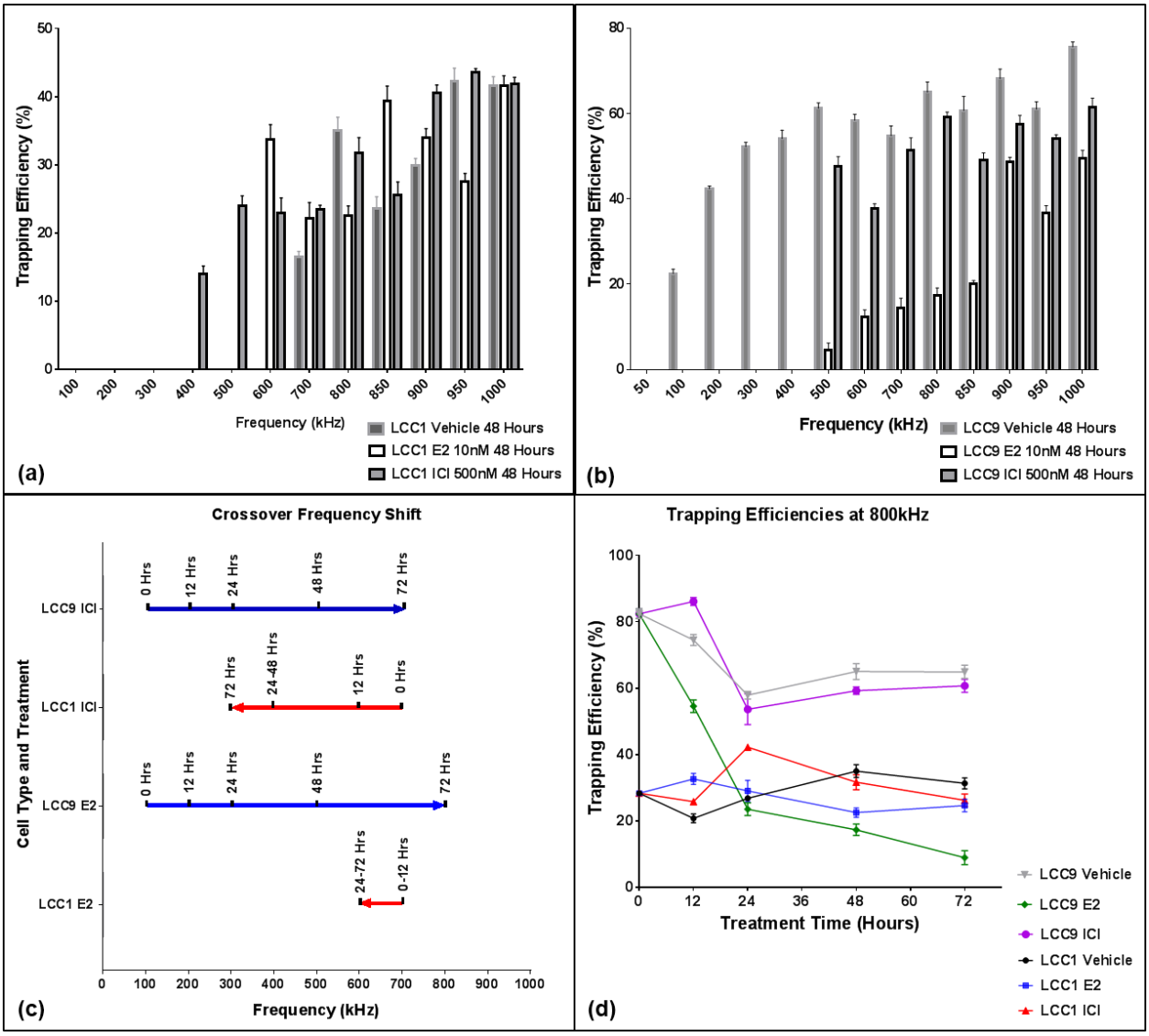

Figure 4-2 (a) Trapping profile of LCC1 and, (b) trapping profile of LCC9 cells for 48 hours of treatment, each point represents mean ± SEM (n>=3), (c) crossover frequency shift for LCC1 and LCC9 cells with ICI and E2 treatment, (d) trapping efficiency comparison of all the experiments at 800kHz, each point represents mean ± SEM (n>=3).

III. Cell Morphology

SEM images of the LCC1 and LCC9 cells after 72 hours of treatment of each of the agents reveal different morphology (Figure 4-3). For LCC1 cells ICI treatment creates a surface with more pores, whereas estrogen treatment does not have a noticeable effect. LCC9 cells treated with ICI show a smoother surface compared to the vehicle, while estrogen treated samples show a different kind of roughness with more pores compared to the vehicle.

Careful inspection of the SEM images of ICI treated cells at different time points reveals a consistent but different behavior in LCC1 and LCC9 cells (Figure 4-4). LCC1 cells do not change much in terms of the surface extrusions, but more pores and voids are observed with increased treatment time. In LCC9 cells, the cells show less roughness and lose their extrusion with increased treatment time.

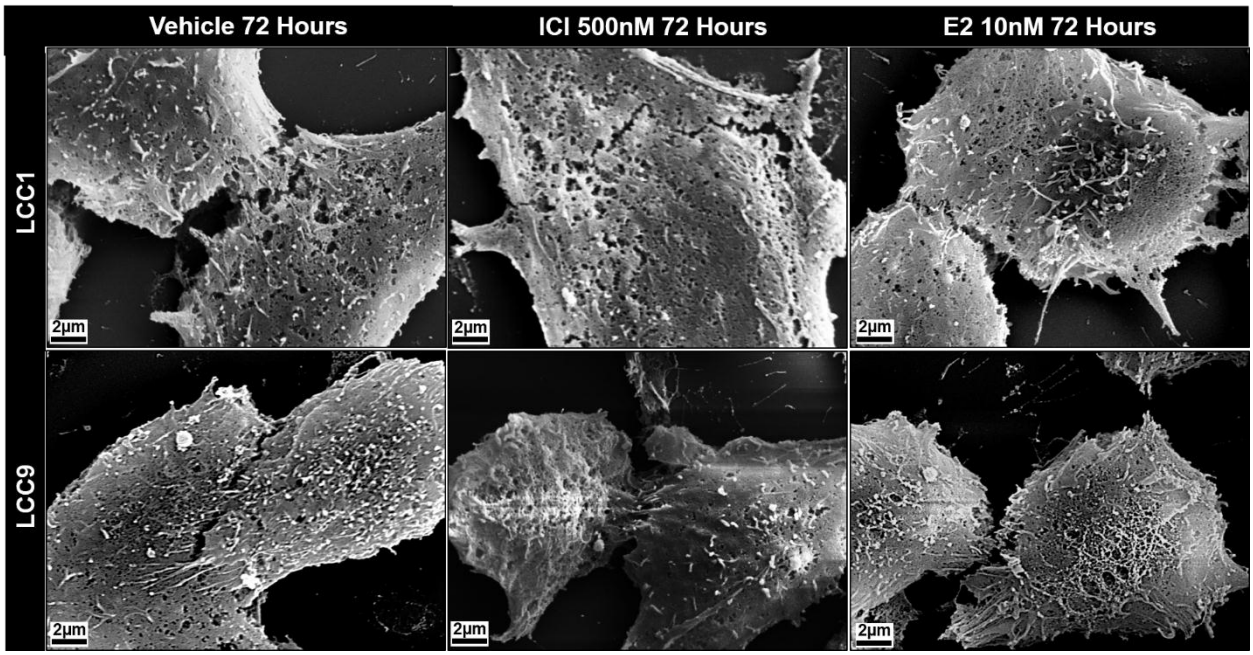

Figure 4-3 SEM images of LCC1 and LCC9 cells after 72 hours of treatment with different agents.

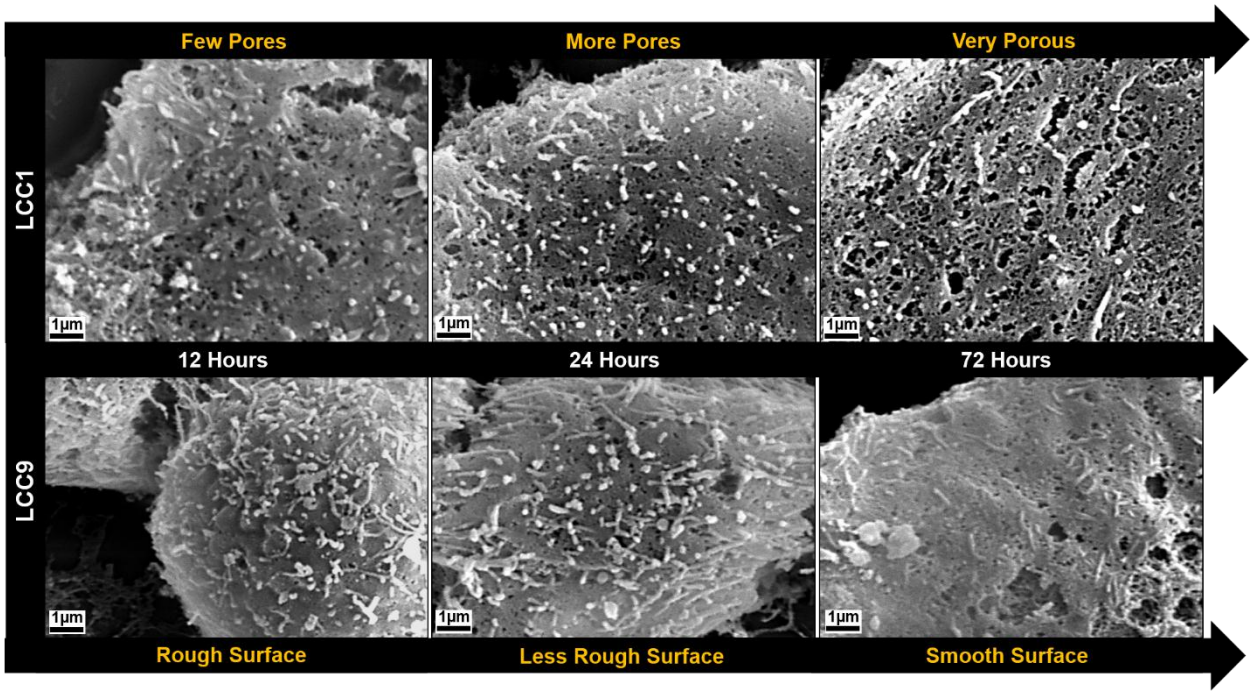

Figure 4-4 SEM images of ICI 500nM treated LCC1 and LCC9 cells over time.

IV. Effect of Treatment on Cell Sizes

Since particle size is a determining factor in the dieletrophoretic force exerted on the cell [60], cell sizes for 72 hour treatments were measured to better understand the acquired dielectrophoretic profiles (Table 2). Based on the results, the cell sizes for the vehicle treatment are very similar to no treatment, indicating the vehicle in not changing the cells in a significant manner. For LCC1 cells, both estrogen and ICI treatments result in the cells becoming larger, whereas LCC9 cells shrink in size with both treatments. This reverse trend in cell size can be one explanation of the reverse behavior observed in the crossover frequency for the two cell lines.

Table 4-2 Measured cell sizes for different treatments.

Treatment	Untreated	Vehicle 72 Hours	ICI500nM 72 Hours	E2 10nM 72 Hours
LCC1 Size (µm)	13.06 ± 1.94	13.38 ±1.84	15.78 ± 2.45	14.13 ± 3.27
LCC9 Size (µm)	14.75 ± 1.25	14.49 ± 1.54	12.45 ± 1.55	11.88 ± 1.42

4.4 Discussion

The dielectrophoresis force acting upon the cell is a factor of various parameters as shown by Pohl [33]. The DEP profile (trapping efficiency in this work) can provide valuable information regarding the electrical properties of the cell. One such information can be extracted from the low crossover frequency which has been observed in the results presented. Based on previously developed models and the fulfillment of certain conditions [63], the low crossover frequency can be expressed as:

Equation 4-1

$$f_{x1} = \frac{\sqrt{2}}{2\pi R C_m}\,\sigma_s$$

Where R is the particle radius, C_m is the membrane capacitance, and σ_s is the conductivity of the solution the cells are suspended in. Based on this equation the crossover frequency has a reverse relationship with both the cell radius and membrane capacitance. Using the cell size measurements and observed frequencies, we can compare the membrane capacitance to the vehicle case. Based on these results, we can observe that higher capacitance relates to less smooth surfaces, either becoming more porous or exhibiting more extrusions on their surface. This phenomenon has been observed in other work [57].

4.5 Conclusion

Using dielectrophoresis as characterization tool we have presented a comprehensive comparison of drug resistance and related mechanisms between different stages of HR^+ cancer cells using LCC1 and LCC9 cell lines as representative models. The dielectrophoresis platform presented in this work has various benefits such as a high throughput sensitive tool which can be further modified to provide separation as well. Moreover, this platform does not have the problem of heating or electrolysis as in contact electrode devices. The separate sample cartridge provides a cost-effective yet simple channel for the sample which can be made as single use part, simplifying experimental protocols and reducing experiment time.

Traditionally drug resistance was considered as the cell not changing when in contact with the drug. However, our results indicate that drug resistance may be more complex with the cell undergoing changes in its structure to prevent the drug from entering the cell.

The different trapping profiles of LCC1 and LCC9 cells envision the possibility of separation between the different strains of drug resistance among a given sample. This can prove beneficial in cases where patients have undergone therapy and need further follow up to make sure resistant strains have not formed in the body, causing the recurrence of cancer. Such a platform can enable the detection of resistant strains, providing the possibility to change to more effective drugs for the patient.

Chapter 5. Summary and Outlook

5.1 Summary of Publications

I. A Microengineered Boyden Chamber for Cell Migration Analysis

In this chapter, we have presented a novel microfabricated Boyden chamber in silicon with well-defined pore sizes and controlled membrane thickness for cell migration analysis. The chip-based chamber is fabricated employing lithography and DRIE techniques on a double-side polished silicon wafer. This microdevice contains micro-pores with a silicon oxide layer at the top and a deep microfluidic channel at the bottom, which is anodically-bonded to a glass wafer for sealing and facilitating the imaging. The applicability of the chip has been demonstrated through the distinct migratory behaviors of highly metastatic breast cancer cells, MDA-MB-231, through pores with 8μm in diameter and 30μm in thickness. Utilizing this micro-based Boyden chamber device, we have shown that MDA-MB-231 cells migrated distinctively in higher rate than MDA-MB-231 cells which had gone through SKI drug treatment over a course of 12 hours.

II. Dielectrophoresis –based Differentiation of Cells

In this chapter we have presented the application of the previously established OπDEP platform for differentiating between different mammalian cell lines. This type kind characterization can provide means for separation and sample enrichment based on the electrical properties of the cell. Moreover, morphology studies have been employed to probe the source of the observed changes in the DEP spectrum. Drug treatment of cells, revealed the effects of the anti-tumor drug GX to hormone responsive breast cancer cells. Therefore, this platform can be used as a drug assessment and discovery tool.

III. Dielectrophoresis as a Cell Characterization and Drug Assessment Tool

In this work, the effect of estrogen and anti-estrogen drug on different strains of hormone responsive breast cancer cells has been explored using dielectrophoresis. Results in this work suggest that contrary to the traditional belief that resistance of a cell to a drug is equivalent to the cell not changing is not accurate. The results confirm that the phenomenon of drug resistance is a complex process which may include various cell changes to create such a resistance. Careful

inspection of the membrane properties of the cell, also reveal that many structural changes are occurring at the surface which can attribute to the different DEP profile as well. This platform can be further modified to include separation of target cells as well.

5.2 Future Work and Outlook

The future of the presented work can rely on the improvement and modification of the transmigration assay discussed in chapter 2. The implementation of this assay on a silicon substrate is beneficial for future modifications such as creating gradient profiles of the size and/or distribution of the pores, since the fabrication techniques utilized in this work are highly controllable and customizable. Additionally, the compatibility of silicon with microfabrication techniques will enable us to perform label-free detection of cell migration by integrating electrodes and sensing elements on this platform. Furthermore, microfluidics and microchannels on this device can be easily modified to create the desired chemical gradient profiles. In future, we hope to further miniaturize this platform to reduce the amount of reagents and samples needed while providing a means for high throughput assays. In addition, we will enhance the functionality of this device by adding electrodes and creating a label-free method for cell migration sensing and test other drug treatment plans with this enhanced platform.

Furthermore, the designed transmigration assay can be combined with the dielectrophoresis platform to do serial analysis of samples. Assume we are looking for resistant types of cancer cells in a patient derived sample. Based on our initial characterizations, we will be able to define a set of characteristics for resistant strains using the OπDEP platform. Therefore, the first step of this serial analysis would be to trap and separate resistant strains in a sample using DEP. Thereafter the extracted cells can be fed into the transmigration assay to check if any of the drug resistant types are exhibiting invasive and metastatic behavior, rendering the use of stronger drugs necessary in order to overcome and treat the resistant strain in the patient.

References

[1] P. S. Dittrich and A. Manz, "Lab-on-a-chip: microfluidics in drug discovery," *Nat Rev Drug Discov,* vol. 5, pp. 210-8, Mar 2006.

[2] R. L. Siegel, K. D. Miller, and A. Jemal, "Cancer statistics, 2016," *CA Cancer J Clin,* vol. 66, pp. 7-30, Jan-Feb 2016.

[3] Y. Tang, Y. Wang, M. F. Kiani, and B. Wang, "Classification, Treatment Strategy, and Associated Drug Resistance in Breast Cancer," *Clin Breast Cancer,* May 13 2016.

[4] F. Tomao, A. Papa, E. Zaccarelli, L. Rossi, D. Caruso, M. Minozzi, *et al.*, "Triple-negative breast cancer: new perspectives for targeted therapies," *Onco Targets Ther,* vol. 8, pp. 177-93, 2015.

[5] "Cancer Facts & Figures 2014," *American Cancer Society,* 2014.

[6] I. J. Fidler, "The pathogenesis of cancer metastasis: the 'seed and soil' hypothesis revisited," *Nature Reviews Cancer,* vol. 3, pp. 453–8, Jun 2003.

[7] P. Friedl and K. Wolf, "Tumour-cell invasion and migration: diversity and escape mechanisms," *Nature Reviews Cancer,* vol. 3, pp. 362–74, May 2003.

[8] P. Friedl and K. Wolf, "Plasticity of cell migration: a multiscale tuning model," *Journal of Cell Biology,* vol. 188, pp. 11–19, Jan 11 2010.

[9] R. R. Balcarcel and L. M. Clark, "Metabolic screening of mammalian cell cultures using well-plates," *Biotechnology Progress,* vol. 19, pp. 98–108, Jan-Feb 2003.

[10] M. Zhao, H. Bai, E. Wang, J. V. Forrester, and C. D. McCaig, "Electrical stimulation directly induces pre-angiogenic responses in vascular endothelial cells by signaling through VEGF receptors," *Journal of Cell Science,* vol. 117, pp. 397–405, Jan 26 2004.

[11] S. I. Fraley, Y. Feng, R. Krishnamurthy, D. H. Kim, A. Celedon, G. D. Longmore, *et al.*, "A distinctive role for focal adhesion proteins in three-dimensional cell motility," *Nature Cell Biology,* vol. 12, pp. 598–604, Jun 2010.

[12] W. L. Chen, K. T. Kuo, T. Y. Chou, C. L. Chen, C. H. Wang, Y. H. Wei, *et al.*, "The role of cytochrome c oxidase subunit Va in non-small cell lung carcinoma cells: association with migration, invasion and prediction of distant metastasis," *BMC Cancer,* vol. 12, p. 273, 2012.

[13] R. Harisi, I. Kenessey, J. N. Olah, F. Timar, I. Babo, G. Pogany, *et al.*, "Differential inhibition of single and cluster type tumor cell migration," *Anticancer Research,* vol. 29, pp. 2981–5, Aug 2009.

[14] S. Qi, Y. Song, Y. Peng, H. Wang, H. Long, X. Yu, *et al.*, "ZEB2 mediates multiple pathways regulating cell proliferation, migration, invasion, and apoptosis in glioma," *PLoS One,* vol. 7, p. e38842, 2012.

[15] G. J. Todaro, G. K. Lazar, and H. Green, "The initiation of cell division in a contact-inhibited mammalian cell line," *Journal of Cellular Physiology,* vol. 66, pp. 325–33, Dec 1965.

[16] C. C. Liang, A. Y. Park, and J. L. Guan, "In vitro scratch assay: a convenient and inexpensive method for analysis of cell migration in vitro," *Nature Protocols,* vol. 2, pp. 329–33, 2007.

[17] S. Krueger, T. Kalinski, H. Wolf, U. Kellner, and A. Roessner, "Interactions between human colon carcinoma cells, fibroblasts and monocytic cells in coculture--regulation of cathepsin B expression and invasiveness," *Cancer Letters,* vol. 223, pp. 313–22, Jun 8 2005.

[18] M. Vinci, C. Box, M. Zimmermann, and S. A. Eccles, "Tumor spheroid-based migration assays for evaluation of therapeutic agents," *Methods in Molecular Biology*, vol. 986, pp. 253–66, 2013.
[19] R. D. Systems. (2016). *Cell Invasion Assays: R&D Systems*. Available: https://www.rndsystems.com/products/cell-invasion-assays
[20] S. Chung, R. Sudo, P. J. Mack, C. R. Wan, V. Vickerman, and R. D. Kamm, "Cell migration into scaffolds under co-culture conditions in a microfluidic platform," *Lab on a Chip*, vol. 9, pp. 269–75, 2009.
[21] I. K. Zervantonakis, S. K. Hughes-Alford, J. L. Charest, J. S. Condeelis, F. B. Gertler, and R. D. Kamm, "Three-dimensional microfluidic model for tumor cell intravasation and endothelial barrier function," *Proceedings of the National Academy of Sciences of the United States of America*, vol. 109, pp. 13515–20, Aug 21 2012.
[22] J. S. Jeon, I. K. Zervantonakis, S. Chung, R. D. Kamm, and J. L. Charest, "<italic>In Vitro</italic> Model of Tumor Cell Extravasation," *PLoS ONE*, vol. 8, p. e56910, 2013.
[23] M. B. Chen, S. Srigunapalan, A. R. Wheeler, and C. A. Simmons, "A 3D microfluidic platform incorporating methacrylated gelatin hydrogels to study physiological cardiovascular cell-cell interactions," *Lab On a Chip*, vol. 13, pp. 2591–8, Jul 7 2013.
[24] S. Bersini, J. S. Jeon, G. Dubini, C. Arrigoni, S. Chung, J. L. Charest, *et al.*, "A microfluidic 3D in vitro model for specificity of breast cancer metastasis to bone," *Biomaterials*, vol. 35, pp. 2454–61, Mar 2014.
[25] K. E. Sung, N. Yang, C. Pehlke, P. J. Keely, K. W. Eliceiri, A. Friedl, *et al.*, "Transition to invasion in breast cancer: a microfluidic in vitro model enables examination of spatial and temporal effects," *Integrative Biology*, vol. 3, pp. 439–50, Apr 2011.
[26] T. Liu, C. Li, H. Li, S. Zeng, J. Qin, and B. Lin, "A microfluidic device for characterizing the invasion of cancer cells in 3-D matrix," *Electrophoresis*, vol. 30, pp. 4285–91, Dec 2009.
[27] K. C. Chaw, M. Manimaran, E. H. Tay, and S. Swaminathan, "Multi-step microfluidic device for studying cancer metastasis," *Lab On a Chip*, vol. 7, pp. 1041–7, Aug 2007.
[28] M. Vinci, S. Gowan, F. Boxall, L. Patterson, M. Zimmermann, W. Court, *et al.*, "Advances in establishment and analysis of three-dimensional tumor spheroid-based functional assays for target validation and drug evaluation," *Bmc Biology*, vol. 10, Mar 2012.
[29] J. N. Heck, S. M. Ponik, M. G. Garcia-Mendoza, C. A. Pehlke, D. R. Inman, K. W. Eliceiri, *et al.*, "Microtubules regulate GEF-H1 in response to extracellular matrix stiffness," *Molecular Biology of the Cell*, vol. 23, pp. 2583-92, Jul 2012.
[30] K. Wolf and P. Friedl, "Mapping proteolytic cancer cell-extracellular matrix interfaces," *Clinical & Experimental Metastasis*, vol. 26, pp. 289-98, Apr 2009.
[31] M. Sameni, D. Cavallo-Medved, J. Dosescu, C. Jedeszko, K. Moin, S. R. Mullins, *et al.*, "Imaging and quantifying the dynamics of tumor-associated proteolysis," *Clinical & Experimental Metastasis*, vol. 26, pp. 299-309, Apr 2009.
[32] V. Brekhman and G. Neufeld, "A novel asymmetric 3D in-vitro assay for the study of tumor cell invasion," *Bmc Cancer*, vol. 9, Nov 2009.
[33] H. A. Pohl, "The Motion and Precipitation of Suspensoids in Divergent Electric Fields," *Journal of Applied Physics*, vol. 22, pp. 869-871, 1951.
[34] M. Li, W. H. Li, J. Zhang, G. Alici, and W. Wen, "A review of microfabrication techniques and dielectrophoretic microdevices for particle manipulation and separation," *Journal of Physics D: Applied Physics*, vol. 47, p. 063001, 2014.

[35] A. Irimajiri, T. Hanai, and A. Inouye, "A dielectric theory of “multi-stratified shell” model with its application to a lymphoma cell," *Journal of Theoretical Biology,* vol. 78, pp. 251-269, 1979/05/21 1979.
[36] R. Pethig, "Review Article—Dielectrophoresis: Status of the theory, technology, and applications," *Biomicrofluidics,* vol. 4, p. 022811, 2010.
[37] A. Salamanzadeh and R. V. Davalos, "Chapter 3. Electrokinetics and Rare-Cell Detection," pp. 61-83, 2014.
[38] E. Primiceri, M. S. Chiriaco, F. Dioguardi, A. G. Monteduro, E. D'Amone, R. Rinaldi, *et al.*, "Automatic transwell assay by an EIS cell chip to monitor cell migration," *Lab on a Chip,* vol. 11, pp. 4081–6, 2011.
[39] D. Kwasny, K. Kiilerich-Pedersen, J. Moresco, M. Dimaki, N. Rozlosnik, and W. E. Svendsen, "Microfluidic device to study cell transmigration under physiological shear stress conditions," *Biomedical Microdevices,* vol. 13, pp. 899–907, Oct 2011.
[40] M. Koyanagi, T. Fukushima, and T. Tanaka, "High-Density Through Silicon Vias for 3-D LSIs," *Proceedings of the IEEE,* vol. 97, pp. 49–59, Jan 2009.
[41] D. S. Tezcan, K. De Munck, N. Pham, O. Luhn, A. Aarts, P. De Moor, *et al.*, "Development of vertical and tapered via etch for 3D through wafer interconnect technology," in *8th Electronic Packaging Technology Conference*, 2006, pp. 22–8.
[42] H. Shakeel and M. Agah, "Semipacked Separation Columns with Monolayer Protected Gold Stationary Phases for Microgas Chromatography," in *Proceedings of the IEEE Sensors* 2012, pp. 2007–10.
[43] A. Zeniou, K. Ellinas, A. Olziersky, and E. Gogolides, "Ultra-high aspect ratio Si nanowires fabricated with plasma etching: plasma processing, mechanical stability analysis against adhesion and capillary forces and oleophobicity," *Nanotechnology,* vol. 25, Jan 24 2014.
[44] K. S. Chen, A. A. Ayon, X. Zhang, and S. M. Spearing, "Effect of process parameters on the surface morphology and mechanical performance of silicon structures after deep reactive ion etching (DRIE)," *Journal of Microelectromechanical Systems,* vol. 11, pp. 264–75, Jun 2002.
[45] K. Gantz, L. Renaghan, and M. Agah, "Development of a comprehensive model for RIE-lag-based three-dimensional microchannel Fabrication," *Journal of Micromechanics and Microengineering,* vol. 18, p. 025003, 2008.
[46] K. J. French, R. S. Schrecengost, B. D. Lee, Y. Zhuang, S. N. Smith, J. L. Eberly, *et al.*, "Discovery and Evaluation of Inhibitors of Human Sphingosine Kinase," *Cancer Research,* vol. 63, pp. 5962–9, 2003.
[47] K. J. French, J. J. Upson, S. N. Keller, Y. Zhuang, J. K. Yun, and C. D. Smith, "Antitumor Activity of Sphingosine Kinase Inhibitors," *Journal of Pharmacology and Experimental Therapeutics,* vol. 318, pp. 596–603, 2006.
[48] Y. Lv, L. Zeng, G. Zhang, Y. Xu, Y. Lu, K. Mitchelson, *et al.*, "Systematic dielectrophoretic analysis of the Ara-C-induced NB4 cell apoptosis combined with gene expression profiling," *Int J Nanomedicine,* vol. 8, pp. 2333-50, 2013.
[49] P. R. Gascoyne and S. Shim, "Isolation of circulating tumor cells by dielectrophoresis," *Cancers (Basel),* vol. 6, pp. 545-79, 2014.
[50] H. M. Coley, F. H. Labeed, H. Thomas, and M. P. Hughes, "Biophysical characterization of MDR breast cancer cell lines reveals the cytoplasm is critical in determining drug sensitivity," *Biochim Biophys Acta,* vol. 1770, pp. 601-8, Apr 2007.

[51] P. Zellner, T. Shake, A. Sahari, B. Behkam, and M. Agah, "Off-chip passivated-electrode, insulator-based dielectrophoresis (OpiDEP)," *Anal Bioanal Chem,* vol. 405, pp. 6657-66, Aug 2013.
[52] J. L. Schwartz-Roberts, A. N. Shajahan, K. L. Cook, A. Warri, M. Abu-Asab, and R. Clarke, "GX15-070 (obatoclax) induces apoptosis and inhibits cathepsin D- and L-mediated autophagosomal lysis in antiestrogen-resistant breast cancer cells," *Mol Cancer Ther,* vol. 12, pp. 448-59, Apr 2013.
[53] P. R. C. Gascoyne, S. Shim, J. Noshari, F. F. Becker, and K. Stemke-Hale, "Correlations between the dielectric properties and exterior morphology of cells revealed by dielectrophoretic field-flow fractionation," *ELECTROPHORESIS,* vol. 34, pp. 1042-1050, 2013.
[54] D. Nakidde, P. Zellner, M. M. Alemi, T. Shake, Y. Hosseini, M. V. Riquelme, *et al.*, "Three dimensional passivated-electrode insulator-based dielectrophoresis," *Biomicrofluidics,* vol. 9, p. 014125, Jan 2015.
[55] K. F. Hoettges, J. W. Dale, and M. P. Hughes, "Rapid determination of antibiotic resistance in E. coli using dielectrophoresis," *Phys Med Biol,* vol. 52, pp. 6001-9, Oct 7 2007.
[56] C. C. Chung, I. F. Cheng, W. H. Yang, and H. C. Chang, "Antibiotic susceptibility test based on the dielectrophoretic behavior of elongated Escherichia coli with cephalexin treatment," *Biomicrofluidics,* vol. 5, p. 21102, Jun 2011.
[57] X. Wang, F. F. Becker, and P. R. Gascoyne, "Membrane dielectric changes indicate induced apoptosis in HL-60 cells more sensitively than surface phosphatidylserine expression or DNA fragmentation," *Biochimica et Biophysica Acta,* vol. 1564, pp. 412-420, 2002.
[58] H. J. Mulhall, A. Cardnell, K. F. Hoettges, F. H. Labeed, and M. P. Hughes, "Apoptosis progression studied using parallel dielectrophoresis electrophysiological analysis and flow cytometry," *Integr Biol (Camb),* vol. 7, pp. 1396-401, Nov 2015.
[59] R. Pethig, A. Menachery, S. Pells, and P. De Sousa, "Dielectrophoresis: a review of applications for stem cell research," *J Biomed Biotechnol,* vol. 2010, p. 182581, 2010.
[60] L. M. Broche, F. H. Labeed, and M. P. Hughes, "Extraction of dielectric properties of multiple populations from dielectrophoretic collection spectrum data," *Phys Med Biol,* vol. 50, pp. 2267-74, May 21 2005.
[61] C. Chou, J. O. Tegenfeldt, O. Bakajin, S. S. Chan, E. C. Cox, N. Darnton, *et al.*, "Electrodeless Dielectrophoresis of Single- and Double-Stranded DNA," *Biophysical Journal,* vol. 83, pp. 2170-2179, 2003.
[62] E. B. Cummings and A. K. Singh, "Dielectrophoresis in Microchips Containing Arrays of Insulating Posts: Theoretical and Experimental Results," *Analytical Chemistry,* vol. 75, pp. 4724-4731, 2003.
[63] R. Pethig and M. S. Talary, "Dielectrophoretic detection of membrane morphology changes in Jurkat T-cells undergoing etoposide-induced apoptosis," *IET Nanobiotechnol,* vol. 1, pp. 2-9, Feb 2007.